Identifying Optimal Machine Learning Approaches for Human Gut Microbiome (Shotgun Metagenomics) and Metabolomics Integration with Stable Feature Selection

Suzette N. Palmer[1-3*], Animesh Mishra[1,4], Shuheng Gan[3], Dajiang Liu[5], Andrew Y. Koh[1,4,6], Xiaowei Zhan[3,6*]

Author information:

[1]Division of Hematology/Oncology, Department of Pediatrics, The University of Texas Southwestern Medical Center, Dallas, TX 75390, USA

[2]Department of Biomedical Engineering, The University of Texas Southwestern Medical Center, Dallas, TX 75390, USA

[3]Peter O'Donnell Jr. School of Public Health, Quantitative Biomedical Research Center, Center for the Genetics and Host Defense, The University of Texas Southwestern Medical Center, Dallas, TX 75390, USA

[4]Department of Microbiology, The University of Texas Southwestern Medical Center, Dallas, TX 75390, USA

[5]Department of Public Health Sciences, Pennsylvania State University College of Medicine, Hershey, PA 17033, USA

[6]Harold C. Simmons Comprehensive Cancer Center, The University of Texas Southwestern Medical Center, Dallas, TX 75390, USA

Contributions

S.N.P., A.Y.K., and X.Z. planned the research; S.N.P. performed the experiments; S.N.P. analyzed the data; A.M. and S.G. contributed technical support. S.N.P., A.M., X.Z., D.L., and A.Y.K wrote the paper.

*Corresponding authors

Correspondence to Xiaowei Zhan at xiaowei.zhan@utsouthwestern.edu and/or 214-648-5194.

Keywords: microbiome; metabolomics; multi-omics integration; feature selection; machine learning; benchmarking study; metagenomics

Abstract

Microbiome research has been limited by methodological inconsistencies. Taxonomy-based profiling presents challenges such as data sparsity, variable taxonomic resolution, and the reliance on DNA-based profiling, which provides limited functional insight. Multi-omics integration has emerged as a promising approach to link microbiome composition with function. However, the lack of standardized methodologies and inconsistencies in machine learning strategies has hindered reproducibility. Additionally, while machine learning can be used to identify key microbial and metabolic features, the stability of feature selection across models and data types remains underexplored, despite its importance for downstream experimental validation and biomarker discovery. Here, we systematically compare Elastic Net, Random Forest, and XGBoost across five multi-omics integration strategies: Concatenation, Averaged Stacking, Weighted Non-negative Least Squares (NNLS), Lasso Stacking, and Partial Least Squares (PLS), as well as individual omics models. We evaluate performance across 588 binary and 735 continuous models using human gut microbiome-derived metabolomics and taxonomic data derived from metagenomics shotgun sequencing data. Additionally, we assess the impact of feature reduction on model performance and feature selection stability. Among the approaches tested, Random Forest combined with NNLS yielded the highest overall performance across diverse datasets. Tree-based methods also demonstrated consistent feature selection across data types and dimensionalities. These results demonstrate how integration strategies, algorithm selection, data dimensionality, and response type impact both predictive performance and the stability of selected features in multi-omics microbiome modeling.

Key Points

- A total of 1,323 models were developed to comprehensively evaluate prediction performance and the robustness of feature selection for human gut microbiome (metabolomics and taxonomy from metagenomics shotgun sequencing) datasets. These models included three widely used machine learning algorithms – Elastic Net, Random Forest and XGBoost – applied across five integration strategies and single-omics approaches on datasets with binary and continuous outcomes.
- For continuous outcomes, Random Forest combined with NNLS integration achieved the highest performance and maintained strong predictive performance across full-dimensional and feature-reduced datasets.
- For binary outcomes, Random Forest consistently performed well regardless of the integration strategy. Notably, single-omics models, especially those using metabolomics data, outperformed integrative approaches.
- Tree-based models demonstrated greater consistency in feature selection across different dimensionalities and integration strategies.

Introduction

The gut microbiome plays a critical role in host homeostasis and is implicated in the development of various diseases [1,2]. However, microbiome research has largely relied on correlative studies, with limited reproducibility due to methodological discrepancies and data-specific challenges [3–5]. Most microbiome studies focus on taxonomy-based profiling (e.g., 16S rRNA sequencing, metagenomic shotgun sequencing), which introduces challenges such as 1) data sparsity (i.e., a large proportion of zeros representing absent taxa), 2) varying levels of taxonomic resolution, and 3) reliance on DNA-based profiling, which does not necessarily reflect functional microbial activity, such as metabolite or protein production [6,7]. These limitations hinder efforts to move beyond association-based findings toward mechanistic insights.

To address these challenges, multi-omics integration — which combines taxonomic data with functional omics (e.g., metabolomics, proteomics, transcriptomics) — has emerged as a promising strategy for uncovering disease-relevant microbial interactions [8–10]. Integrative approaches increase analytical power, allowing researchers to link microbiome composition with functional microbial activity. However, microbiome research methodologies vary widely in data processing, resolution, and integration strategies [11–16] (**Supplemental File 1**). The lack of standardized methodologies can lead to inconsistencies in microbiome-derived findings [17–19]. Differences in machine learning models and integration strategies can yield highly variable results, making it difficult to establish reproducible biomarkers or validate disease associations across studies [10,20,21]. Without a systematic evaluation of these methods, it remains unclear which approaches provide the most biologically meaningful and clinically translatable insights.

To address these gaps, we conducted a multi-faceted analysis to evaluate performance trends and feature selection stability across various multi-omics data integration techniques. Specifically, we analyzed 4 human gut microbiome multi-omics datasets with matched microbiome (metagenomic shotgun sequencing) and metabolomics data and assessed integration performance for both binary and continuous outcomes. Our analysis applied Random Forest, XGBoost, and Elastic Net models to both full-dimensional and feature-reduced datasets. We compared model performance across single-omics and multi-omics approaches, focusing on two integration strategies: concatenation and stacked generalization. For stacked generalization, we implemented Averaged Stacking, Weighted Non-Negative Least Squares (NNLS) [22], Lasso Stacking (LS) [23], and Partial

82 Least Squares (PLS) [24]. To evaluate the impact of dimensionality reduction, we filtered and reduced features
83 within each omics dataset and compared model performance against the full-dimensional datasets (**Figure 1A**,
84 **Tables 1–2**) [11,14,25,26]. Subsequently, we assessed the performance of concatenation, stacked
85 generalization, and single-omics models (**Figure 1B**). Finally, we examined feature selection consistency across
86 machine learning models and integration strategies, comparing stability between single-omics and concatenated
87 approaches (**Figure 1C**).

88 **Results**

89 **Creation of integrative analysis pipeline to analyze continuous and binary datasets**

90 We collected and processed four multi-omics datasets consisting of matched metagenomic shotgun
91 sequencing and metabolomics data, and we evaluated 18 continuous and 13 binary matching response
92 variables (**Table 1-2**) [11,14,25,26]. The decision to use certain covariates as response variables was guided
93 by their relevance to the disease or their known relation to microbial and metabolite differences in populations.
94 We included BMI [27,28], Age [29], Gender [30-31], Alcohol usage [32], and Brinkman Index [33] based on
95 prior links to perturbations in the gut microbiome and/or metabolites. For Gastrectomy, Glucose and Total
96 Cholesterol were chosen due to alterations in microbiome and metabolome profiles [34,35,36]. For IBD, Fecal
97 Calprotectin was used since it is a marker of inflammation and was measured and correlated in the original
98 study with Irritable Bowel Disease (IBD) [11]. For Renal failure, Creatinine, eGFR, and Urea were included as
99 clinical markers of disease, and prior studies have shown that renal failure is associated with altered
100 metabolome and microbiome [37,38]. For Yachida (Colorectal Cancer), we also evaluated subsets of the
101 diseases, separating them by different stages of cancer when compared to control. For the Franzosa (IBD)
102 datasets, we developed models based on subtypes (Ulcerative Colitis (UC) or Chron's Disease (CD)), as well
103 as the entire IBD group.

104 We then developed an integrative analysis pipeline to assess the performance of three machine
105 learning algorithms (Elastic Net, Random Forest, XGBoost) in combination with five integration approaches
106 (Concatenated, Averaged Stacked (AS), Weighted Non-negative Least Squares (NNLS), Lasso Stacked (LS),
107 and Partial Least Squares (PLS). For concatenation, the metabolomics and metagenomic abundances for

each matched sample were appended to form a single long feature vector that served as input for the analysis. The remaining four approaches relied on stacked generalization, where separate base models were first trained on the metabolomics data and on the metagenomics data. The out-of-fold predictions from the two base models were stacked to form two meta-features, which were combined by a meta-learner using all four strategies: AS, NNLS, LS, and PLS (**Figure 1A-B**). We evaluated each stacking approach on feature-reduced and full-dimensional datasets to assess how well these models performed under different feature scenarios (**Table 1-2**). Each analysis incorporated a grid search with 3 repeated 5-fold cross validation to optimize the base models, and performance was assessed using root mean squared error (RMSE) for continuous outcomes and area under the receiver operating characteristic curve (AUROC) for binary outcomes. Uniform grid parameters were applied across all analyses, and features (or, for stacked models, base model-level importances) were extracted for downstream selection analysis (see **Methods** for more details).

Random Forest with Non-Negative Least Squares Integration Emerges as the Top Performer on Datasets with Continuous Response Variables

We analyzed 364 feature-reduced and 371 full-dimensional models with continuous response variables across 18 datasets using 5 integration approaches and 2 single-omics datasets (Metabolomics, MSS). To assess model performance, we selected the top 3 models (marked as *,**,***, with "*" as the best performing model) for each dataset (**Figure 2**). Random Forest emerged as the top-performing algorithm for feature-reduced (44.1%) and full-dimensional (46.3%) datasets (**Figure 2B-D**). Among integration methods, Non-Negative Least Squares (NNLS) dominated for both feature-reduced (72.2%) and full-dimensional (75.9%) datasets (**Figure 2B, 2D**).

Interestingly, 9 individual metabolomics models and 1 MSS model outperformed several top integration methods in the feature-reduced datasets, with 10 metabolomics models and 1 MSS model showing similar trends in full-dimensional datasets (**Figure 2A**, **2C**). Despite significant feature reduction, performance comparisons between feature-reduced and full-dimensional datasets remained consistent, underscoring the robustness of the Random Forest-NNLS combination for integrating continuous datasets (**Figure 2**).

When examining validation RMSE, weighted NNLS had elevated performance for feature-reduced (40.7%) and full-dimensional (38.9%) datasets and was only outperformed by PLS. However, PLS had severe overfitting (50.0%) with low testing performance (7.4% regardless of dimensionality) (**Figure 2, Supplemental**

135 **Figure 1**). Overall, the Random Forest-NNLS combination consistently delivered superior results for datasets
136 with continuous response variables.

137 **Random Forest Maintains Dominance in Binary Outcome Datasets**

138 We analyzed 217 feature-reduced and 210 full-dimensional models with binary response variables across
139 13 datasets, applying the same integration approaches and machine learning algorithms as the continuous
140 dataset analysis (**Figure 3A**, **Supplemental Figure 2**). Random Forest dominated for both the feature-reduced
141 (84.2%) and full-dimensional datasets (72.7%) (**Figure 3**). For binary datasets, regardless of dimensionality,
142 there seemed to be relatively even distribution of performance despite integration technique with a slight
143 performance majority for AS. The top performing integration strategies for feature-reduced were AS (21.2%) and
144 NNLS (21.2%) (**Figure 3A-B**). The top performing integration strategy for full-dimensional datasets was AS
145 (30.3%) (**Figure 3C-D**).

146 Notably, several single-omics models outperformed the integrative methods in both the feature-reduced
147 and full-dimensional datasets. Among the feature-reduced datasets, 2 metabolomics models and 7 MSS models
148 showed superior performance (**Figure 3A**). In the full-dimensional datasets, 4 metabolomics and 4 MSS models
149 outperformed the integrative approaches (**Figure 3C**). Validation AUROC indicate comparable performance
150 across integration methods, with the exception of PLS (36.1%), which overfit (**Supplemental Figure 2**), similar
151 to the continuous analysis results (**Supplemental Figure 1**). Elastic Net and XGBoost also displayed overfitting,
152 as evidenced by validation AUROC means being higher than testing performance (**Figure 3**, **Supplemental**
153 **Figure 2**). Overall, the Random Forest algorithm demonstrated robustness across all scenarios, irrespective of
154 integration approach (**Figure 2-3**).

155 **Uncovering Trends in Feature Selection Across Elastic Net, Random Forest and XGBoost**

156 Following model development, we next sought to determine whether our base models (Elastic Net,
157 Random Forest, and XGBoost) identified similar features across concatenated and single-omics (Metabolomics
158 and Taxa) datasets (**Figure 1C**). Understanding how different models select features across various dataset
159 conditions (feature-reduced vs. full-dimensional, binary vs. continuous) is crucial for evaluating model
160 consistency and the impact of preprocessing steps on feature selection.

To assess feature selection across models, we first extracted feature importance metrics from each cross-validation step (see **Methods** for more details). For each run, we computed the absolute value of each feature's importance score and applied min-max normalization. This normalization ensures that feature importance values are comparable across models, preventing any single model from dominating due to differences in scale. We then used the mean importance to identify the top overall features for each model. For this analysis, we grouped features into bins based on their importance scores within each model, selecting those with the highest feature importance. To ensure rigor, we used predefined bin sizes, which represent the top 1, 5, 10, 20 and 50 features. These discrete bins create a manageable list of high-priority candidates that can be feasibly validated through peer review, or experimentally through *in vivo* and *in vitro* studies. These predefined list sizes also allowed us to compare the most influential features across models without the impractical task of vetting each variable across every dataset. Violin plots are used for the following analysis to depict the distribution of the proportions of features selected that are shared and/or unique across Elastic Net, Random Forest and XGBoost for each dataset.

Metabolite Features Selected by Tree-Based Methods Show Strong Concordance, in Contrast to the Distinct Features Selected by Elastic Net

We examined metabolite feature-selection patterns from Elastic Net, Random Forest, and XGBoost in feature-reduced and full-dimensional datasets with binary and continuous response variables (**Figure 4A**). Across conditions, Elastic Net consistently identified a large proportion of unique features, regardless of dimensionality, response type, or bin size (**Figure 4B-E**).

Overlap among the top-ranked features chosen by all three models was minimal (**Figure 4B-E**). In nearly every dataset, the top feature differed; only one reduced continuous dataset (**Figure 4B**) and two full-dimensional binary datasets (**Figure 4E**) showed any common top feature. Another clear pattern was the near-absence of agreement between Elastic Net and the tree-based models when features were binned from 5-50. In these larger bins, overlapping metabolites typically accounted for less than one-quarter of the selections across every dataset, dimensionality and response type considered. The only exception occurred in the reduced continuous metabolomics set, where overlap between Elastic Net and both Random Forest and XGBoost for several datasets reached ~40 % for the top five features (**Figure 4B**).

By contrast, Random Forest and XGBoost showed substantially higher concordance. Violin plots demonstrated that these two models consistently shared a stable subset of metabolites across bin sizes 1–50, independent of outcome type or dataset dimensionality (**Figure 4**). Dimensionality reduction marginally increased three-way agreement for continuous data (**Figure 4B-C**) but had little effect on binary response types. Taken together, tree-based models tend to agree on a core group of features, whereas Elastic Net repeatedly favors distinct selections.

Tree-Models Reveal Partial Concordance in Taxa Selection While Elastic Net Remains Distinct

To evaluate taxa feature selection, we analyzed full-dimensional and feature-reduced datasets with binary or continuous outcomes (**Figure 5A**). Similar to the metabolite analysis, there were no cases where the three models converged on the same top-ranked taxa. Additionally, Elastic Net never shared its top feature with either Random Forest or XGBoost (**Figure 5B-E**).

Patterns for the tree-based methods varied with response type. For continuous outcomes, Random Forest and XGBoost agreed on the top feature more often in full-dimensional than in reduced datasets (**Figure 5B-C**). For binary outcomes the opposite was true, with higher top feature concordance after dimensionality reduction (**Figure 5D-E**). In bins 5–50, violin plots showed that roughly half of all selected taxa were common to both tree-based models, while the remainder were uniquely assigned to one or the other (**Figure 5B-E**). Violin plots showed similar distributions of shared taxa between Random Forest and XGBoost, which closely mirrored those of their unique selections. These indicated that each algorithm still identified a considerable number of distinct taxa, even under scenarios of higher concordance. Elastic Net behaved distinctly from the tree-based methods, and across bins 1–50, more than 75% of the top features selected were unique for most datasets (**Figure 5B-E**).

Distinct Elastic Net Selections Contrast with Consistent Tree-Based Features for Concatenated Models

We next studied concatenated models that jointly analyze metabolite and taxa features (**Figure 6A**). For continuous outcomes, the patterns resembled the taxa-only feature analysis. There was only one instance of agreement for the top feature selected across all three algorithms, which occurred in the feature-reduced continuous dataset (**Figure 6B**).

Elastic Net almost never overlapped with the tree-based methods. A single continuous dataset shared the top feature between Elastic Net and XGBoost, and none showed overlap between Elastic Net and Random

Forest (**Figure 6B-E**). Conversely, Random Forest and XGBoost continued to display notable concordance, sharing approximately half of their top-ranked features for datasets with binary and continuous outcomes. Examining larger bins (5–50) reinforced this pattern. Shared-feature proportions among all three models, or between Elastic Net and either tree-based method, rarely exceeded 25%. Random Forest and XGBoost typically shared close to 50% concordance (**Figure 6B-E**).

Dimensionality Reduction Influences Feature Selection Stability in Machine Learning Models

To evaluate the impact of dimensionality reduction on model behavior, we compared feature selection between full-dimensional and feature-reduced datasets for Elastic Net, Random Forest, and XGBoost across all metabolomics, taxa, and concatenated datasets using binary and continuous response variables (**Figure 7A**). Our goal was to determine whether dimensionality affected feature-selection stability and whether the top features selected remained consistent across the different machine learning algorithms.

Across all data types and response variables, Elastic Net consistently demonstrated minimal agreement in top-feature selection for the full-dimensional and feature-reduced models (**Figure 7B-G**). Regardless of whether the dataset involved metabolomics, taxonomy, or concatenated data, or the response type, only 1–2 datasets showed overlap in the top feature selected by Elastic Net (**Figure 7B-G**). In contrast, the tree-based models, with greater emphasis on Random Forest, showed stronger consistency in the top features selected for the metabolomics datasets (**Figure 7B, 7E**). Approximately half of the Random Forest models identified the same top feature in both the full and feature-reduced datasets for both binary and continuous response variables. XGBoost followed a similar trend for metabolomics data, with slightly lower proportions of agreement in top features (**Figure 7B, 7E**).

In contrast, for taxa and concatenated datasets, top-feature agreement between full-dimensional and reduced models was rare, even for the tree-based methods (**Figure 7C-D, 7F-G**). Across these analyses, Random Forest and XGBoost typically shared the same top feature in only 1–4 datasets, indicating that dimensionality reduction substantially influences which features are prioritized for these data types (**Figure 7C-D, 7F-G**).

When examining bins 5–50, further insights emerged regarding the broader set of selected features. For metabolomics data, regardless of response type, the majority of datasets showed less than 50% overlap in features between the full-dimensional and feature-reduced Elastic Net models (**Figure 7B, 7E**). Most distributions for Elastic Net were centered around zero and displayed major differences in selected features. Notably, Random Forest models applied to metabolomics datasets demonstrated relatively even distributions of overlap across bins 5–50, while XGBoost distributions differed based on response type (**Figure 7B, 7E**). For continuous outcomes, XGBoost showed a concentration of overlapping proportions in the 0.0–0.20 range, whereas binary outcomes exhibited a more even spread across all feature bins (**Figure 7B, 7E**).

For taxa data, feature overlap across bins 5–50 for Elastic Net was sparse, with the highest density of violin-plot distributions concentrated at zero for both binary and continuous response types (**Figure 7C, 7F**). Some exceptions were observed, one continuous taxa dataset at bin 5 and two binary taxa datasets at bin 5, which showed complete agreement in selected features between full and reduced models (**Figure 7C, 7F**). Random Forest models developed using taxa data showed a more evenly distributed pattern of overlap, whereas XGBoost had the largest distribution near zero but still demonstrated higher concordance than Elastic Net across most bins (**Figure 7C, 7F**).

Trends observed in the concatenated models closely mirrored those seen in the taxa data (**Figure 7D, 7G**). However, distributions for bins 5–50 were generally shifted closer to zero across all three modeling approaches, indicating even lower agreement in selected features between full-dimensional and feature-reduced models (**Figure 7D, 7G**). This suggests that when combining multiple data types, feature selection becomes increasingly sensitive to dimensionality, especially for Elastic Net, which consistently demonstrated the least concordance between full and feature-reduced models.

Dimensionality and Data Integration Lead to Divergent Feature Selection

To determine whether concatenated models which incorporate both metabolomics and taxa data could recover features identified by single-omics models, we compared feature-selection patterns across Elastic Net, Random Forest, and XGBoost for both full-dimensional and feature-reduced datasets with continuous and binary response types (**Figure 8A, 8F**). In the feature-reduced and full-dimensional datasets, there was limited

agreement between the concatenated and metabolomics Elastic Net models for continuous outcomes, with most overlap proportions falling below 0.4 and the highest dataset density occurring near zero (**Figure 8B-C**). For binary outcomes regardless of dimensionality, Elastic Net was unable to recover any overlapping features with between the concatenated and metabolomics models (**Figure 8D-E**).

In contrast, the Random Forest and XGBoost models more effectively identified overlapping metabolites between concatenated and metabolomics single-omics datasets (**Figure 8B–E**). Within the top 50 feature bins, both models consistently recovered shared metabolites, and in several datasets, the same leading features were selected. For continuous outcomes, these features showed comparable distributions between full-dimensional and reduced datasets (**Figure 8B–C**).

When comparing taxa features between concatenated and single-omics models, we observed a higher degree of consensus relative to the metabolite comparisons. Elastic Net models, surprisingly, displayed substantial overlap across all bins, with the majority of feature-overlap proportions falling in the 0.75 to 1.0 range across both full-dimensional and feature-reduced datasets, regardless of response type (**Figure 8G-J**). An exception occurred in the top-feature comparison for the full-dimensional binary dataset, where only one dataset showed agreement between the concatenated and taxa models (**Figure 8J**).

For Random Forest and XGBoost, the proportion of overlapping taxa features between concatenated and single-omics datasets remained proportional across feature bins 5–50, regardless of feature dimensionality (**Figure 8G-J**). Slightly less agreement was observed in the top feature selection for datasets with continuous responses when compared with binary, where the latter demonstrated higher and more proportionate overlap (**Figure 8G-J**).

To further investigate how different data types influence model behavior for concatenated data, we evaluated the proportion of taxa versus metabolite features selected across bin sizes 1–50 (**Supplemental Figure 3A**). For Elastic Net, taxa consistently dominated feature selection across all datasets, with top features in every bin originating from the taxa data, regardless of dimensionality or response type (**Supplemental Figure 3B-E**). This suggests Elastic Net may be more sensitive to high-dimensional features within concatenated models. By contrast, the feature sets chosen by Random Forest and XGBoost displayed a more

293 even metabolite-to-taxon ratio across dimensionality bins, suggesting that these ensemble methods are less
294 sensitive to changes in dimensionality (**Supplemental Figure 3B-E**).

295 **Discussion**

296 This study presents a comprehensive evaluation of machine learning performance and feature selection
297 stability across multi-omics microbiome and metabolomics datasets using Elastic Net, Random Forest and
298 XGBoost. By systematically comparing these models across both continuous and binary response variables,
299 full-dimensional and feature-reduced datasets, and integration strategies including concatenation and ensemble-
300 based methods, we aimed to uncover generalizable trends in model behavior and feature selection stability
301 (**Figure 1**). One of the most consistent findings was the robust performance of Random Forest, particularly when
302 combined with Non-Negative Least Squares (NNLS) integration, for datasets with continuous outcomes (**Figure**
303 **2**). This is consistent with prior studies highlighting the capacity of Random Forest to effectively handle noisy,
304 sparse, nonlinear and high dimensional data, such as microbiome data [5,39,40]. NNLS further enhanced model
305 performance, reinforcing recent evidence that integration methods leveraging weighted combinations of
306 predictions can outperform simpler or more complex stacking strategies for microbiome multi-omics data [16].

307 Across binary outcomes, Random Forest also outperformed other models, though the advantage was
308 less pronounced with more comparable performances across the stacked integration methods (**Figure 3**).
309 Notably, several single-omics models outperformed integrative models for both binary and continuous
310 responses, particularly metabolomics models. This suggests that in certain cases, single-omics models may
311 identify strong predictive features and/or relationships that are lost during integration. We also observed that
312 model performance results were largely consistent between full-dimensional and feature-reduced datasets, with
313 Random Forest maintaining top performance across both response types (**Figure 2-3**). This suggests that,
314 despite substantial reductions in input features, overall predictive performance can be preserved when robust
315 models and integration strategies are applied [41].

316 In terms of feature selection, a key trend that emerged across all datasets is that Elastic Net consistently
317 identified a distinct and largely non-overlapping set of features compared to Random Forest and XGBoost
318 (**Figure 4-6**). This divergence is likely attributable to the linear and sparsity-inducing nature of Elastic Net, which
319 tends to select a small subset of features that are linearly associated with the outcome and includes groups of

correlated predictors. Alternatively, tree-based models are more adept at capturing nonlinear, higher-order interactions and distributed signals [42].

This trend was particularly evident in the metabolomics datasets, where Random Forest and XGBoost frequently shared more than 50% of their top-ranked features across bins, while Elastic Net consistently selected a largely distinct set of features (**Figure 4**). The divergence in feature selection became even more pronounced in the concatenated models that combined metabolomics and taxonomic data (**Figures 5–6**). Feature selection stability was also more sensitive to dimensionality, with Elastic Net showing minimal overlap in top-ranked features between full and feature-reduced datasets, especially in metabolomics, whereas Random Forest and XGBoost demonstrated moderate consistency (**Figure 7**). These findings suggest that dimensionality reduction alters the feature landscape more substantially for linear models, and that feature interpretability and reproducibility in Elastic Net may be more influenced by preprocessing choices compared to tree-based approaches.

When comparing feature selection between single-omics and concatenated models, tree-based methods retained a relatively high degree of consistency, while Elastic Net rarely recovered the same features—especially in metabolomics analyses (**Figure 8**). Interestingly, for taxonomic features, Elastic Net showed much higher agreement between concatenated and single-omics models. This pattern likely reflects higher dimensionality in the concatenated datasets, where taxa features outnumber metabolite features. As a result, Elastic Net appears biased towards selecting taxa features, while Random Forest and XGBoost maintained a more balanced selection across both data types. These results are consistent with previous findings suggesting that tree-based models are more resilient to greater numbers of features and sparsity in high-dimensional data [42].

While this work provides several new insights into model behavior and feature selection for microbiome multi-omics data, there are several limitations. First, the study was conducted using four multi-omics microbiome datasets [11,14,25,26], limiting generalizability. Broader applications across a wider range of microbiome-related diseases would help validate these findings. Additionally, taxonomic profiling was performed using Kracken v2.1.1 and Bracken v2.8, which may produce different results when compared to other classification tools [43,44]. We also only selected one method for feature reduction analyses. We used Limma [45] for metabolomics data

346 and Wilcoxon signed-rank test for the taxonomic relative abundance data. These might not be the best methods
347 for feature reduction and/or may not accurately reflect feature signal structure across all datasets. Exploration
348 into other methods of microbiome data transformation and its effect on multi-omics data integration should be
349 explored [46].

350 Furthermore, the concatenated datasets suffered from greater dimensionality, with taxa feature
351 outnumbering metabolomics for all datasets. This imbalance likely contributed to Elastic Net's consistent
352 selection of taxa-only features. Finally, a uniform hyperparameter grid was used across all models, which
353 provided standardization but may not have captured optimal tuning for individual datasets. Future works should
354 incorporate additional datasets exploring diverse diseases, consider additional integration methods such as
355 DIABLO [47] or MOFA+ [48], explore alternative dimensionality reduction strategies and taxa classification
356 strategies and include refined hyperparameter optimization. Additionally, biological validation of selected
357 features, through literature mining or experimental follow-up, is crucial to ensure biological relevance. Overall,
358 this study offers a robust framework for evaluating machine learning performance and feature selection in multi-
359 omics microbiome data, highlighting the strengths and limitations of current modeling strategies and laying the
360 groundwork for more interpretable and scalable integrative analysis.

361 **Methods**

362 Data Collection and Processing

363 The data used in this study were originally obtained from Franzosa et al. (2019) [11], Yachida et al. (2019) [14],
364 Erawijantari et al. (2020) [25], and Wang et al. (2020) [26]. Processed taxonomy relative abundance and
365 metabolomics processed data were obtained from Muller et al. (2022) [49]. Details can also be found at
366 https://github.com/borenstein-lab/microbiome-metabolome-curated-data/wiki5 and in **Supplemental File 2**.

367 Data Processing for the Integrated Analysis

368 Processed data files for metabolomics, metadata, species level relative abundance and genus level relative
369 abundance were further processed for downstream analysis. Taxonomic data at the genus and species levels
370 were concatenated for each dataset, and taxa with an overall abundance across samples that was less than
371 0.1% were removed. For metabolite differential intensity analysis, Limma 3.64.1 [45] was applied, which employs
372 linear modeling and empirical Bayes methods to identify significant differences while adjusting for multiple testing

373 using Benjamini-Hochberg procedure. For taxonomic differential analysis, the Wilcoxon rank-sum test was used
374 to compare taxa abundance across experimental groups (More details in **Supplemental File 2**).

375 Overview of Multi-omics Integrative Analysis

376 The integrative analysis was developed using a custom in-house script that is readily available at
377 https://github.com/suziepalmer10/Multiomics-Integrative-Pipeline/tree/main. The packages tidyverse 2.0.0 and
378 argparse 2.2.3 were used to parse and pre-process the data for this integrative analysis [50]. For continuous
379 outcomes, performance was assessed with Root Mean Squared Error (RMSE), and binary classification was
380 evaluated using the Area Under the Receiver Operating Characteristic Curve (AUROC). For the integrative
381 analysis, AUROC is calculated using pROC 1.18.0 [51].

382 For this analysis, each dataset (as described above, in **Supplemental File 2,** and presented in **Tables**
383 **1–2**) was processed through the Integrated Pipeline using Elastic Net, Random Forest, and XGBoost scripts.
384 The data was split into 80% training and 20% testing, and three repeats of five-fold cross-validation were
385 performed. To ensure both generalizability and reproducibility, the random seed for each fold was set by
386 multiplying the repeat index and the fold index (**Supplemental File 2**). Performance was evaluated on validation
387 and test sets. Grid search with a predefined grid was used for Elastic Net, Random Forest, and XGBoost
388 (**Supplemental File 2**).

389 Selection of Machine Learning Methods and Integrative Strategies: Elastic Net, Random Forest, and XGBoost
390 were chosen because they have been widely used in microbiome research for building predictive models and
391 identifying features for experimental validation [52-54]. For multi-omics integration, we used direct
392 concatenation and stacked generalization, two approaches frequently used in this field [11–16]. Collectively,
393 these algorithms and integration techniques offer interpretable models that can be readily validated through
394 literature review and experimental follow-up (see **Supplemental File 1** for more details).

395 Machine-learning Algorithm Overview: A detailed description of each algorithm is provided in **Supplemental**
396 **File 2**. Elastic Net models were implemented with the caret v 6.0-93 and glmnet v 4.1-6 R packages [23, 55].
397 Random Forest models used caret and randomForest v 4.7-1.1 packages [55,56], and XGBoost models were
398 built with caret and xgboost v 1.7.8.1 [55,57].

399 Data Integration Overview. A detailed description of each method is described in **Supplemental File 2**. Direct
400 concatenation was performed by vertically stacking the metabolomics and taxa matrices and fitting a single
401 model to the combined feature set. In averaged stacking (AS), predictions from separate models trained on
402 each data type were averaged to yield a single prediction. Weighted non-negative least-squares (NNLS)
403 integration combined base-model predictions by learning non-negative weights that minimized prediction error
404 and was implemented using the nnls package v 1.5 [22]. LASSO integration estimates a linear combination of
405 the base-model predictions by minimizing squared error plus an L_1 penalty on the weights and was
406 implemented with glmnet v 4.1-6 [23]. Partial least squares (PLS) integration applied PLS regression to the
407 base predictors with the pls package v 2.8-4 [24].

408 Model Performance Visualization: Mean RMSE and AUROC values were displayed using the
409 ComplexHeatmap package [58,59]. The three best performing models for each dataset are denoted by one (*),
410 two (**), or three (***) asterisks. Pie charts summarizing how often each algorithm or integration method ranked
411 in the top three were generated with ggplot2 (see **Supplemental File 2** for additional details) [60].

412 Feature Extraction:

413 Feature importance values were extracted from Elastic Net, XGBoost and Random Forest across all 15 cross-
414 validation models. Since different metrics were used to quantify feature importance across Elastic Net, Random
415 Forest and XGBoost models, we decided to take the absolute value of each variable and perform min-max
416 normalization (data scaled between 0 and 1) for each model, which allows for direct comparison between
417 features in each model (See **Supplemental File 2** for more details).

418 For this analysis, the number of top features selected per model was determined by varying feature bin
419 sizes of 1, 5, 10, 20 and 50. For each bin size, only the top n features (where n equals the bin size) were retained
420 to represent the most important features. The features contained in each bin have the greatest importance values
421 and represent the top features that might be explored using peer review and/or by experimentation. Violin plots
422 were generated using ggplot2 to illustrate the overlap and uniqueness of features selected by Elastic Net,
423 Random Forest and XGBoost [60]. The proportions of overlapping and unique features for each dataset are

424 represented as individual circles within a violin plot. Models with fewer than n feature ranked above 0, or those
425 that were not able to finish, were excluded from the analysis.

426 **Data Availability**

427 Data is free and available through: https://github.com/borenstein-lab/microbiome-metabolome-curated-
428 data/wiki/Data-overview#datasets-included [49]. Code for this integrative analysis and associated analysis are
429 free and available through: https://github.com/suziepalmer10/Multiomics-Integrative-Pipeline.

430 **Funding**

431 This work is supported by National Institute of Allergy and Infectious Disease [grant numbers AI179406 to A.Y.K.,
432 AI169298 to X.Z., 5T32AI005284-43 to S.N.P.]; the University of Texas Southwestern Medical Center and
433 Children's Health Cellular and ImmunoTherapeutics Program (to A.Y.K.); National Human Genome Research
434 Institute [grant number HG011035 to D.L.]; and National Institute of General Medical Sciences [grant number
435 GM126479 to X.Z.].

436 **Competing Interests**

437 AYK is a consultant for Prolacta Bioscience. AYK receives research funding from Novartis. AYK is co-founder of
438 Aumenta Biosciences.

439

References

1. Gilbert JA, Quinn RA, Debelius J, et al. Microbiome-wide association studies link dynamic microbial consortia to disease. Nature. 2016 Jul 7;535(7610).
2. Joos R, Boucher K, Lavelle A, et al. Examining the healthy human microbiome concept. Nature Reviews Microbiology. 2024 Mar;23(3):192-205.
3. Walter J, Armet AM, Finlay BB, et al. Establishing or Exaggerating Causality for the Gut Microbiome: Lessons from Human Microbiota-Associated Rodents. Cell. 2020 Jan 23;180(2):221-232.
4. Corander J, Hanage WP, Pensar J. Causal discovery for the microbiome. The Lancet Microbe. 2022 Nov;3(11):e881-e887.
5. Knight R, Vrbanac A, Taylor BC, et al. Best practices for analysing microbiomes. Nature Reviews Microbiology. 2018 Jul;16(7):410-422.
6. Galloway-Peña J, Hanson B. Tools for Analysis of the Microbiome. Digestive Diseases and Sciences. 2020 Mar;65(3):674-685.
7. Song EJ, Lee ES, Nam YD. Progress of analytical tools and techniques for human gut microbiome research. Journal of Microbiology. 2018 Oct;56(10):693-705.
8. Hasin Y, Seldin M, Lusis A. Multi-omics approaches to disease. Genome Biology. 2017 May;83(18).
9. Chetty A, Blekhman R. Multi-omic approaches for host-microbiome data integration. Gut Microbes. 2024 Jan-Dec;16(1):2297860.
10. Li P, Luo H, Ji B, et al. Machine learning for data integration in human gut microbiome. Microbial Cell Factories. 2022 Nov 23;21(1):241.
11. Franzosa EA, Sirota-Madi A, Avila-Pacheco J, et al. Gut microbiome structure and metabolic activity in inflammatory bowel disease. Nature Microbiology. 2019 Feb;4(2):293-305.
12. Li J, Zhao F, Wang Y, et al. Gut microbiota dysbiosis contributes to the development of hypertension. Microbiome. 2017 Feb 1;5(1):14.
13. Gao B, Duan Y, Lang S, et al. Functional Microbiomics Reveals Alterations of the Gut Microbiome and Host Co-Metabolism in Patients With Alcoholic Hepatitis. Hepatology Communications. 2020 Jun 19;4(8):1168-1182.
14. Yachida S, Mizutani S, Shiroma H, et al. Metagenomic and metabolomic analyses reveal distinct stage-specific phenotypes of the gut microbiota in colorectal cancer. Nature Medicine. 2019 Jun;25(6):968-976.
15. Ghaemi MS, DiGiulio DB, Contrepois K, et al. Multiomics modeling of the immunome, transcriptome, microbiome, proteome and metabolome adaptations during human pregnancy. Bioinformatics. 2019 Jan 1;35(1):95-103.
16. Mallick H, Porwal A, Saha S, et al. An integrated Bayesian framework for multi-omics prediction and classification. Statistics in Medicine. 2024 Feb 28;43(5):983-1002.
17. Liu YX, Qin Y, Chen T, et al. A practical guide to amplicon and metagenomic analysis of microbiome data. Protein & Cell. 2021 May;12(5):315-330.
18. Poussin C, Sierro N, Boué S, et al. Interrogating the microbiome: experimental and computational considerations in support of study reproducibility. Drug Discovery Today. 2018 Sep;23(9):1644-1657.
19. Huttenhower C, Finn RK, McHardy AC. Challenges and opportunities in sharing microbiome data and analyses. Nature Microbiology. 2023 Nov;8(11):1960-1970.
20. Santiago-Rodriguez TM, Hollister EB. Multi 'omic data integration: A review of concepts, considerations, and approaches. Seminars in Perinatology. 2021 Oct;45(6):151456.
21. Papoutsoglou G, Tarazona S, Lopes MB, et al. Machine learning approaches in microbiome research: challenges and best practices. Frontiers in Microbiology. 2023 Sep 22;14:1261889.
22. Mullen KM, van Stokkum IHM. nnls: The Lawson-Hanson Algorithm for Non-Negative Least Squares (NNLS). https://rdrr.io/cran/nnls/ (27 June 2025, date last accessed).
23. Friedman J, Hastie T, Tibshirani R. et al. Regularization Paths for Generalized Linear Models via Coordinate Descent. Journal of Statistical Software. 2010 Aug;33(1):1-22.
24. Mevik B-H, Wehrens R. The pls Package: Principal Component and Partial Least Squares Regression in R. Journal of Statistical Software. 2007 Jan;18:1–23.
25. Erawijantari PP, Mizutani S, Shiroma H, et al. Influence of gastrectomy for gastric cancer treatment on faecal microbiome and metabolome profiles. Gut. 2020 Aug;69(8):1404-1415.
26. Wang X, Yang S, Li S, et al. Aberrant gut microbiota alters host metabolome and impacts renal failure in humans and rodents. Gut. 2020 Dec;69(12):2131-2142.

27. Ottosson F, Brunkwall L, Ericson U, et al. Connection between BMI-related plasma metabolite profile and gut microbiota. J Clin Endocrinol Metab. 2018 Apr;103(4):1491-1501.
28. Puljiz Z, Kumric M, Vrdoljak J, et al. Obesity, gut microbiota, and metabolome: from pathophysiology to nutritional interventions. Nutrients. 2023 May 9;15(10):2236.
29. Ghosh TS, Shanahan F, O'Toole PW. The gut microbiome as a modulator of healthy ageing. Nat Rev Gastroenterol Hepatol. 2022 Sep;19(9):565-584.
30. Costanzo M, Caterino M, Sotgiu G, et al. Sex differences in the human metabolome. Biol Sex Differ. 2022 Jun 15;13(1):30.
31. Kim YS, Unno T, Kim BY, et al. Sex differences in gut microbiota. World J Mens Health. 2020 Jan;38(1):48-60.
32. Engen PA, Green SJ, Voigt RM, et al. The gastrointestinal microbiome: alcohol effects on the composition of intestinal microbiota. Alcohol Res. 2015;37(2):223-236.
33. Antinozzi M, Giffi M, Sini N, et al. Cigarette smoking and human gut microbiota in healthy adults: a systematic review. Biomedicines. 2022 Feb 21;10(2):510.
34. Maksimaityte V, Bausys A, Kryzauskas M, et al. Gastrectomy impact on the gut microbiome in patients with gastric cancer: a comprehensive review. World J Gastrointest Surg. 2021 Jul 27;13(7):678-688.
35. Lee JW, Kim EY, Yoo HM, et al. Changes of lipid profiles after radical gastrectomy in patients with gastric cancer. Lipids Health Dis. 2015 Mar 21;14:21.
36. Kaska L, Sledzinski T, Chomiczewska A, et al. Improved glucose metabolism following bariatric surgery is associated with increased circulating bile acid concentrations and remodeling of the gut microbiome. World J Gastroenterol. 2016 Oct 21;22(39):8698-8719.
37. Ragi N, Sharma K. Deliverables from metabolomics in kidney disease: adenine, new insights, and implication for clinical decision-making. Am J Nephrol. 2024;55(4):421-438.
38. Tang Z, Yu S, Pan Y. The gut microbiome tango in the progression of chronic kidney disease and potential therapeutic strategies. J Transl Med. 2023 Oct 3;21(1):689.
39. Hernández Medina R, Kutuzova S, Nielsen KN, et al. Machine learning and deep learning applications in microbiome research. ISME Communications. 2022 Oct 6;2(1):98.
40. Kumar B, Lorusso E, Fosso B, et al. A comprehensive overview of microbiome data in the light of machine learning applications: categorization, accessibility, and future directions. Frontiers in Microbiology. 2024 Feb 13;15:1343572.
41. Saeys Y, Inza I, Larrañaga P. A review of feature selection techniques in bioinformatics. Bioinformatics. 2007 Oct 1;23(19):2507-17.
42. Díaz-Uriarte R, Alvarez de Andrés S. Gene selection and classification of microarray data using random forest. BMC Bioinformatics. 2006 Jan 6;7:3.
43. Wood DE, Lu J, Langmead B. Improved metagenomic analysis with Kraken 2. Genome Biology. 2019 Nov 28;20(1):257.
44. Lu J, Breitwieser FP, Thielen P, et al. Bracken: estimating species abundance in metagenomics data. PeerJ Computer Science. 2017 Jan;3:e104.
45. Ritchie ME, Phipson B, Wu D, et al. Limma powers differential expression analyses for RNA-sequencing and microarray studies. Nucleic Acids Research. 2015 Apr 20;43(7):e47.
46. Karwowska Z, Aasmets O; Kosciolek T, et al. Effects of data transformation and model selection on feature importance in microbiome classification data. Microbiome. 2025 Jan 4;13(1):2.
47. Singh A, Shannon CP, Gautier B, et al. DIABLO: an integrative approach for identifying key molecular drivers from multi-omics assays. Bioinformatics. 2019 Sep 1;35(17):3055-3062.
48. Argelaguet R, Arnol D, Bredikhin D, et al. MOFA+: a statistical framework for comprehensive integration of multi-modal single-cell data. Genome Biology. 2020 May 11;21(1):111.
49. Muller E, Algavi YM, Borenstein E. The gut microbiome-metabolome dataset collection: a curated resource for integrative meta-analysis. Npj Biofilms and Microbiomes. 2022 Oct 15;8(1):79.
50. Wickham H, Averick M, Bryan J, et al. Welcome to the Tidyverse. Journal of Open Source Software. 2019 Nov; 4(43):1686.
51. Robin X, Turck N, Hainard A, et al. PROC: an open-source package for R and S+ to analyze and compare ROC curves. BMC Bioinformatics. 2011 Mar 17;12:77.
52. Greener JG, Kandathil SM, Moffat L, et al. A guide to machine learning for biologists. Nature Reviews Molecular Cell Biology. 2022 Jan;23(1):40-55.

53. Li Y, Wu FX, Ngom A. A review on machine learning principles for multi-view biological data integration. Briefings in Bioinformatics. 2018 Mar 1;19(2):325-340.
54. Ghannam RB, Techtmann SM. et al. Machine learning applications in microbial ecology, human microbiome studies, and environmental monitoring. Computational and Structural Biotechnology Journal. 2021 Jan 27;19:1092-1107.
55. Kühn M. Building Predictive Models in R Using the caret Package. Journal of Statistical Software. 2008 Nov;28(5):1-26.
56. Liaw A, Wiener MC. Classification and Regression by randomForest. R News. 2002 Dec;2:18-22.
57. Chen T, Guestrin C. XGBOOST: A Scalable Tree Boosting System. KDD '16: Proceedings of the 22nd ACM SIGKDD International Conference on Knowledge Discovery and Data Mining. 2016 Aug 13; 785-794.
58. Gu Z. Complex heatmap visualization. iMeta. 2022 Sept;3(1):e43.
59. Gu Z, Eils R, Schlesner M. Complex heatmaps reveal patterns and correlations in multidimensional genomic data. Bioinformatics. 2016 Sep 15;32(18):2847-9.
60. Valero-Mora PM, Valero-Mora PM. Ggplot2: Elegant Graphics for Data Analysis. Journal of Statistical Software, Book of Reviews. 2010 Jul;35(1):1-3.

Table 1: Details for Data With Continuous Response Variables

			Featured-Reduced Details					Full-Dimensional Details				
					Run Time (HH:MM)					Run Time (HH:MM)		
Study Name (Subset)	Response Variable	Sample Size	Number of Metabolites	Number of Taxa	Elastic Net	Random Forest	XGBoost	Number of Metabolites	Number of Taxa	Elastic Net	Random Forest	XGBoost
Erawijantari	Age	96	71	775	00:09	00:01	01:55	524	3103	00:25	00:05	03:16
Erawijantari	Total Cholesterol	82	71	775	00:09	00:01	01:50	524	3103	00:25	00:06	02:48
Erawijantari	Glucose	84	71	775	00:09	00:01	01:47	524	3103	00:25	00:06	02:40
Franzosa (Control vs. CD)	Age	144	2175	3603	00:30	00:13	04:50	8848	5137	01:34	00:47	09:56
Franzosa (Control vs. CD)	Fecal Calprotectin (Fp)	107	2175	3603	00:30	00:10	04:10	8848	5137	01:06	00:32	06:50
Franzosa (Control vs. IBD)	Age	220	2519	3849	00:39	00:24	06:15	8848	5137	01:18	01:00	10:11
Franzosa (Control vs IBD	Fecal Calprotectin (Fp)	153	2519	3849	00:33	00:16	04:54	8848	5137	01:08	00:42	07:48
Franzosa (Control vs. UC)	Age	132	1268	1816	00:18	00:06	03:43	8848	5137	01:31	00:45	09:25
Franzosa (Control vs. UC)	Fecal Calprotectin (Fp)	88	1268	1816	00:16	00:04	03:01	8848	5137	01:25	00:36	06:33
Wang	Age	287	71	2261	00:13	00:09	03:22	276	5293	00:26	00:26	04:50
Wang	BMI	280	71	2261	-	00:09	03:06	276	5293	00:26	00:27	04:26
Wang	Creatinine	281	71	2261	00:12	00:10	02:49	276	5293	00:25	00:30	04:10
Wang	eGFR	281	71	2261	00:12	00:11	03:37	276	5293	00:25	00:32	05:11
Wang	Urea	281	71	2261	00:13	00:09	03:33	276	5293	00:25	00:27	04:59
Yachida (All Samples)	Age	347	173	1823	00:23	00:11	03:22	450	5770	00:32	00:34	05:27
Yachida (All Samples)	Alcohol	347	173	1823	00:24	00:11	03:43	450	5770	00:31	00:33	05:47
Yachida (All Samples)	BMI	347	173	1823	-	00:11	03:05	450	5770	-	00:35	05:05
Yachida (All Samples)	Brinkman Index	347	173	1823	00:25	00:12	03:41	450	5770	00:32	00:36	05:46

'-' represents models that failed to complete.

Table 2: Details for Data With Binary Response Variables

			Featured-Reduced Details					Full-Dimensional Details				
					Run Time (HH:MM)					Run Time (HH:MM)		
Study Name (Subset)	Response Variable	Sample Size	Number of Metabolites	Number of Taxa	Elastic Net	Random Forest	XGBoost	Number of Metabolites	Number of Taxa	Elastic Net	Random Forest	XGBoost
Erawijantari	No Alcohol vs. Alcohol	96 (47/49)	71	775	00:09	00:01	01:55	524	3103	00:25	00:05	03:16
Erawijantari	Female vs. Male	96 (32/64)	71	775	-	00:04	01:16	524	3103	00:31	00:28	02:14
Erawijantari	Control vs. Gastrectomy	96 (54/42)	71	775	00:11	00:04	01:08	524	3103	00:23	00:27	02:09
Franzosa (Control vs. CD)	Control vs. CD	144 (56/88)	2175	3603	00:38	01:13	02:43	8848	5137	01:52	04:52	05:29
Franzosa (Control vs. IBD)	Control vs. IBD	220 (56/164)	2519	3849	00:54	02:19	03:16	8848	5137	01:48	07:34	05:34
Franzosa (Control vs. UC)	Control vs. UC	132 (56/76)	1268	1816	00:22	00:30	02:07	8848	5137	01:53	04:45	05:21
Wang	Female vs. Male	287 (107/180	71	2261	-	01:03	02:09	276	5293	-	03:49	03:06
Wang	Control vs. Kidney Failure	287 (67/220)	71	2261	00:17	00:50	01:36	276	5293	00:34	03:11	02:29
Yachida (All Samples)	Female vs. Male	347 (143/204	173	1823	00:18	01:08	02:12	450	5770	00:42	05:16	03:39
Yachida (Control vs MP & CRC)	Control vs. MP and CRC	277 (127/150)	173	1823	00:16	00:51	01:58	450	5770	00:35	04:02	03:15
Yachida (Control vs MP & Stage 0)	Control vs. MP & Stage 0 CRC	194 (127/67)	173	1823	00:07	00:09	01:24	450	5770	-	02:28	02:46
Yachida (Control vs Stage 1 & 2)	Control vs. Stage 1 & 2 CRC	196 (127/69)	173	1823	00:05	00:05	01:13	450	5770	-	02:30	02:47
Yachida (Control vs Stage 3 & 4)	Control vs. Stage 3 & 4 CRC	181 (127/54)	173	1823	00:07	00:08	01:15	450	5770	-	02:08	02:34

'-' represents models that failed to complete.

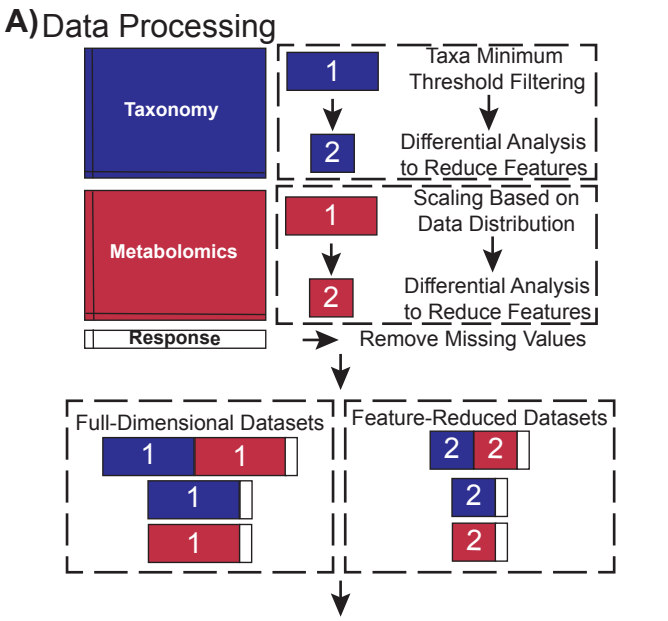

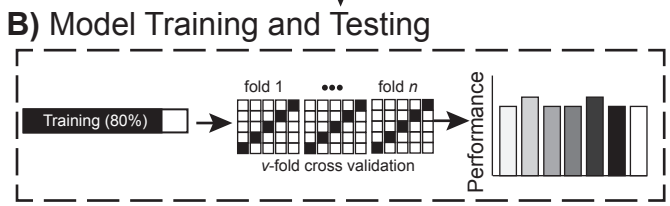

Input Models: Elastic Net, Random Forest, XGBoost
Integration Techniques: Single-omics (Taxonomy and Metabolomics), Concatenatation, Averaged Stacking, Weighted Non-Negative Least Squares (NNLS), Lasso Stacking, Partial Least Squares.

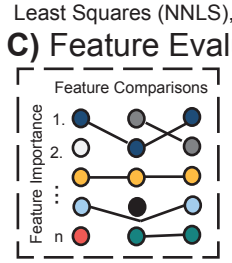

Comparisons:
Elastic Net vs. Random Forest vs. XGBoost
Full-Dimensional vs. Feature-Reduced Datasets
Concatenated vs. Taxonomy/Metabolomics

Figure Legends

Figure 1. Pipeline for the Multi-omics Integrative Analysis. A) Matched taxonomy and metabolomics data are processed separately. Taxa with an abundance below 0.001 across all samples are removed. Depending on the study design and the method used for metabolomics, data are appropriately scaled. Response variables with missing values are excluded from downstream analyses. Differential expression analyses are conducted separately for metabolomics (indicated in red) and taxa (indicated in blue). Both the original datasets (taxa – 1, metabolomics – 1) and their corresponding response variables are concatenated. Similarly, the feature-reduced datasets (taxa – 2, metabolomics – 2) and their response variables are concatenated, enabling comparisons between original and feature-reduced data. **B)** The processed datasets are then analyzed using the multi-omics integration pipeline. The data are first split into 80% training and 20% testing sets. The training data undergo 3 repeat 5-fold cross-validation to optimize model performance. Performance metrics—area under the receiver operating characteristic (ROC) curve (AUROC) for binary outcomes and root mean squared error (RMSE) for continuous outcomes—are used to evaluate both validation and testing performance. The base machine learning models are Elastic Net, XGBoost, and Random Forest. Integration strategies include simple concatenation, averaged stacking, weighted non-negative least squares (NNLS), Lasso stacking, and Partial Least Squares (PLS). Additionally, single-omics models are generated separately for taxonomy and metabolomics datasets. For each response variable, 21 models are generated (or attempted), representing various combinations of base learners, integration methods, and data types. **C)** After model generation, feature extraction is performed. Top features selected by each machine learning model (Elastic Net, Random Forest, XGBoost) are compared to identify consistently important variables. Further comparisons are conducted to assess feature selection differences between full-dimensional and feature-reduced datasets. Lastly, the features selected from concatenated taxonomy and metabolomics base models are compared to those identified in the integrated concatenated models to evaluate the impact of data integration on feature importance.

A) Performance of Feature-Reduced Data with Continuous Response Variables

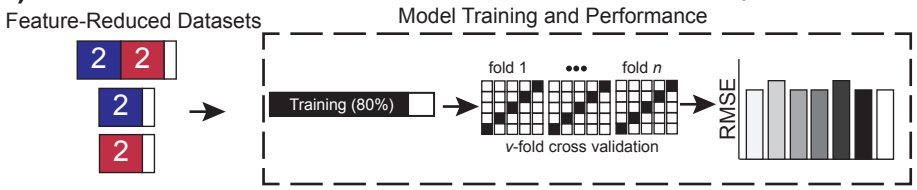

Testing RMSE

$\log_{10}$(RMSE): 3, 2, 1, 0

Model	Dataset	Single-omics: Metab	Single-omics: MSS	Multi-omics Integration: Concat	AS	W-NNLS	LS	PLS
		11.26	21.60	16.89	15.04	10.85**	11.36	11.62
		11.63	11.74	11.63	11.59	11.09***	11.76	12.49
		11.55	13.20	13.12	11.90	10.39*	12.78	13.27
		14.83>*	157.15	138.14	79.39	18.01**	29.80	46.06
		16.98>*	19.61	19.38	17.67*	18.50***	18.98	20.98
		20.43	21.66	21.94	18.68	19.26	20.22	22.14
		12.11	94.64	107.47	49.80	10.99**	13.01	18.21
		11.91	11.39	11.34	11.56	10.95*	11.83	12.97
		13.94	12.46	11.92	12.43	10.99***	12.69	12.94
		13.67	182.15	64.57	90.76	12.56*	14.21	24.54
		13.60	13.54	13.46	13.52	12.96**	13.46	14.14
		14.14	14.57	13.83	13.83	13.16***	13.78	14.08
		1.75	2.46	1.81	1.99	1.70**	1.78	1.88
		1.83	2.04	1.91	1.92	1.73***	1.84	1.90
		1.76	2.23	1.83	1.90	1.68*	1.82	1.87
		15.38>***	106.68	45.96	55.77	15.08*	15.61***	15.95
		16.27	17.10	16.63	16.56	16.08	16.40	17.55
		15.93	17.76	16.84	16.14	15.55**	15.91	16.32
		1.26>***	2.03	1.62	1.52	1.24*	1.28**	1.28***
		1.45	1.78	1.53	1.58	1.37	1.48	1.48
		1.49	1.83	1.53	1.50	1.42	1.49	1.55
		16.84	46.81	51.34	27.74	15.83**	17.40	18.96
		17.82	17.27	17.59	17.32	16.05***	17.40	20.08
		16.49	19.04	18.04	16.98	15.42*	17.41	17.32
		1.49>****	2.56	1.92	1.96	1.28*	1.54	1.45
		1.74	2.19	1.88	1.95	1.36**	1.75	1.63
		1.75	2.11	1.86	1.85	1.52***	1.79	1.84
		11.43	17.46	17.24	12.53	11.15	11.65	12.06
		11.11	10.95	10.90***	10.95	10.86**	10.98	11.30
		11.94	11.22	11.05	11.06	10.85*	11.05	11.04
		3.47	3.54	3.52	3.47	3.38**	3.46***	3.55
		3.81	3.80	3.73	3.61	3.38*	3.67	3.63
		1.39	1.64	1.41	1.39	1.37	1.37	1.44
		0.81	1.19	1.03	0.97	0.63***	0.81	0.66
		0.62>****	1.13	0.71	0.77	0.61*	0.62**	0.64
		39.12	263.71	187.58	133.68	31.88	45.28	46.89
		16.94	28.08	23.80	21.82	10.68*	14.88	12.30
		13.09>****	25.49	16.95	16.47	12.56**	13.34***	13.71
		9.51	37.27	16.47	20.24	9.44	11.28	10.93
		7.55	9.00	8.50	8.14	6.74*	7.42	7.02**
		7.37	8.80	7.61	7.54	7.02***	7.24	7.26
		2.84>****	2.90	2.90	2.85	2.82*	2.85***	2.86
		3.25	3.08	3.09	3.05	2.82**	3.06	2.94
		4.63	4.61	4.61	4.62	4.53	4.63	4.62
		4.46	4.52	4.52	4.45***	4.39*	4.50	4.45**
		4.84	4.61	4.65	4.57	4.47	4.61	4.65
		11.11	17.79	19.95	13.11	10.83	12.36	12.64
		11.35	9.56>****	9.60***	10.31	9.12*	9.74	9.53**
		12.18	10.04	9.88	10.52	10.15	10.31	10.33
		4.20	4.24	4.24	4.21	4.18	4.23	4.43
		4.09>****	4.21	4.21	4.13	4.07**	4.15	4.18
		4.18	4.39	4.27	4.12***	4.03*	4.17	4.17

Row labels: Age; Cholesterol; Glucose; Control vs. CD Age; Control vs. CD Fp; Control vs. IBD Age; Control vs. IBD Fp; Control vs. UC Age; Control vs. UC Fp; Age; BMI; Creatinine; eGFR; Urea; BMI; Brinkman Index; Age; Alcohol

B) Feature-Reduced Categorical Distributions with the Lowest RMSE

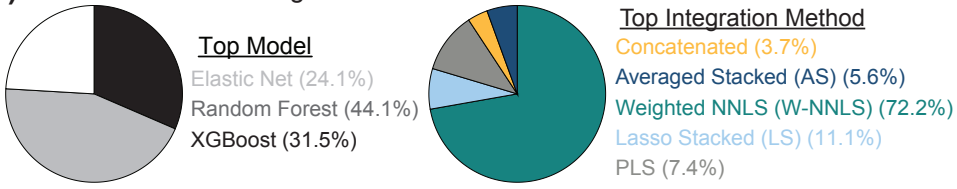

C) Performance of Full-Dimensional Data with Continuous Response Variables

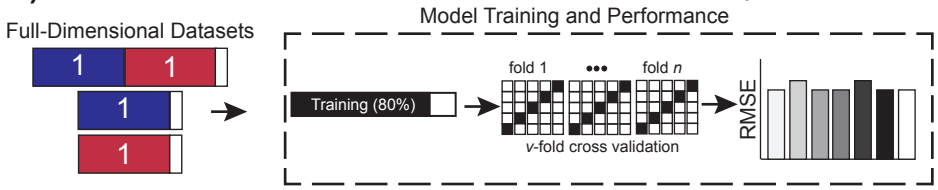

Testing RMSE

$\log_{10}$(RMSE): 4, 3, 2, 1, 0

Dataset: Erawijantari, Franzosa, Wang, Yachida

Model: Elastic Net, Random Forest, XGBoost

Model	Dataset	Single-omics: Metab	Single-omics: MSS	Multi-omics Integration: Concat	AS	W-NNLS	LS	PLS
		10.58>***	582.21	463.18	291.49	10.96***	129.24	104.22
		11.23	11.85	11.75	11.47	10.87**	11.77	12.88
		11.00	12.85	12.48	11.44	10.31*	12.20	12.95
		15.78>**	1536.37	1353.00	768.17	19.32***	229.59	371.82
		18.33>**	20.83	20.32	19.27**	18.96*	19.44	19.85
		21.36	23.55	22.16	20.34	20.29	21.93	24.67
		13.60	841.64	457.05	422.08	10.75**	29.37	119.57
		11.93	12.08	11.94	11.91	10.71*	12.19	13.27
		14.56	13.99	14.61	13.31	10.78***	13.99	12.99
		14.10	287.77	142.76	143.60	13.08***	14.26	16.93
		13.75	13.47	13.58	13.55	13.03**	13.65	14.50
		13.80	13.99	14.02	13.39	12.96*	13.57	13.72
		1.84	2.35	1.99	1.97	1.78*	1.87	1.96
		1.86	2.01	1.88	1.92	1.82***	1.88	2.02
		1.91	2.25	2.01	1.97	1.80**	1.96	2.00
		14.91>***	127.82	39.25	66.16	14.56*	15.15**	15.49
		15.97	17.03	16.22	16.36	15.87	16.23	17.05
		15.88	17.42	16.28	15.92	15.54***	15.86	16.05
		1.36>**	2.03	1.57	1.57	1.34*	1.37***	1.38
		1.49	1.80	1.53	1.62	1.37**	1.51	1.48
		1.51	1.86	1.53	1.53	1.43	1.50	1.63
		15.64>****	142.99	32.77	74.16	15.18*	18.95	27.73
		16.21	17.63	16.60	16.77	15.75***	16.92	20.05
		16.55	18.64	16.61	16.90	15.54**	16.92	17.90
		1.65>****	2.56	1.99	2.00	1.49*	1.69***	1.78
		1.95	2.23	1.99	2.08	1.62**	1.96	1.79
		1.92	2.19	1.90	1.94	1.78	1.92	1.93
		11.70	40.69	39.72	23.70	11.12	11.52	11.58
		10.92	10.82	10.79	10.79	10.65*	10.84	10.93
		11.33	11.09	10.76	10.66***	10.57*	10.85	10.98
		3.53	3.93	3.86	3.67	3.42***	3.57	3.70
		3.49	3.54	3.53	3.49	3.39*	3.48	3.54
		3.69	3.73	3.63	3.54	3.39**	3.59	3.59
		1.28	1.64	1.41	1.36	1.31	1.32	1.36
		0.83	1.24	1.10	1.00	0.65*	0.83	0.68
		0.66>***	1.19	0.71	0.83	0.65**	0.67***	0.70
		28.49	343.64	220.18	171.48	28.70	36.18	41.98
		17.26	29.38	25.61	22.69	10.73*	15.58	12.08**
		13.36	26.22	15.70	17.25	13.26***	14.21	14.85
		9.00	21.85	13.74	13.65	8.96	10.80	10.22
		7.64	9.20	8.76	8.27	6.78*	7.51	7.04***
		7.15	9.19	7.64	7.64	6.85**	7.18	7.22
		2.84>****	2.90	2.90	2.86	2.82**	2.85***	2.86
		3.09	3.03	3.02	2.95	2.82*	2.98	2.90
		4.63	4.61	4.61	4.62	4.53	4.63	4.64
		4.40	4.46	4.45	4.40***	4.26*	4.44	4.33**
		4.61	4.64	4.56	4.47	4.42	4.53	4.54
		11.15	21.82	26.56	15.04	10.88	12.43	12.05
		11.16	9.80>****	9.83	10.37	9.39*	9.83	9.65**
		11.51	9.91	9.99	10.24	9.82***	10.03	10.07
		4.21	4.23	4.23	4.21	4.17	4.22	4.34
		4.09>****	4.21	4.20	4.13***	4.07**	4.15	4.20
		4.18	4.37	4.30	4.14	4.06*	4.14	4.17

Row labels: Age; Cholesterol; Glucose; Control vs. CD Age; Control vs. CD Fp; Control vs. IBD Age; Control vs. IBD Fp; Control vs. UC Age; Control vs. UC Fp; Age; BMI; Creatinine; eGFR; Urea; BMI; Brinkman Index; Age; Alcohol

D) Full-Dimensional Categorical Distributions with the Lowest RMSE

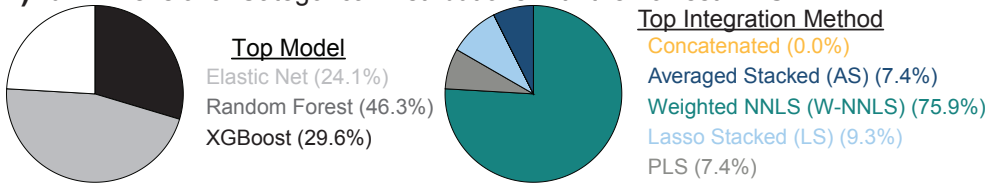

588 **Figure 2. Testing Performance Metrics Across Continuous Feature-Reduced and Full-Dimensional**
589 **Datasets.** Testing performance for feature-reduced matched microbiome and metabolomics datasets with
590 continuous response variables are represented by **A)**. The top performing machine learning models and top
591 integration methods for each of the feature-reduced datasets are represented as pie charts in **B)**. Testing
592 performance for full-dimensional matched microbiome and metabolomics datasets with continuous response
593 variables are represented by **C)**. The top performing machine learning models and top integration methods for
594 each of the full-dimensional datasets are represented as pie charts in **D)**. Performance is assessed using RMSE
595 Mean. Actual RMSE values are shown in each cell of the heatmap with $\log_{10}$ scaling for the coloring. Response
596 variables used for each model are shown on the right of each heatmap. The top performing models per response
597 variable are represented by '*', where '*' is the best performing model, '**' is the second-best performing model
598 and '***' is the third-best performing model. The proportions are calculated using the top three best performing
599 models (*, **, ***) per response variable. 'T' represents ties in performance; response variables with majority 'T'
600 were not used for pie chart calculations. Individual omics (Metabolomics and MSS) were not represented in the
601 pie charts. '>' or 'T' represents increased or tied performance of an individual omics to one of the top performing
602 integration models ('*', '**', and '***').
603

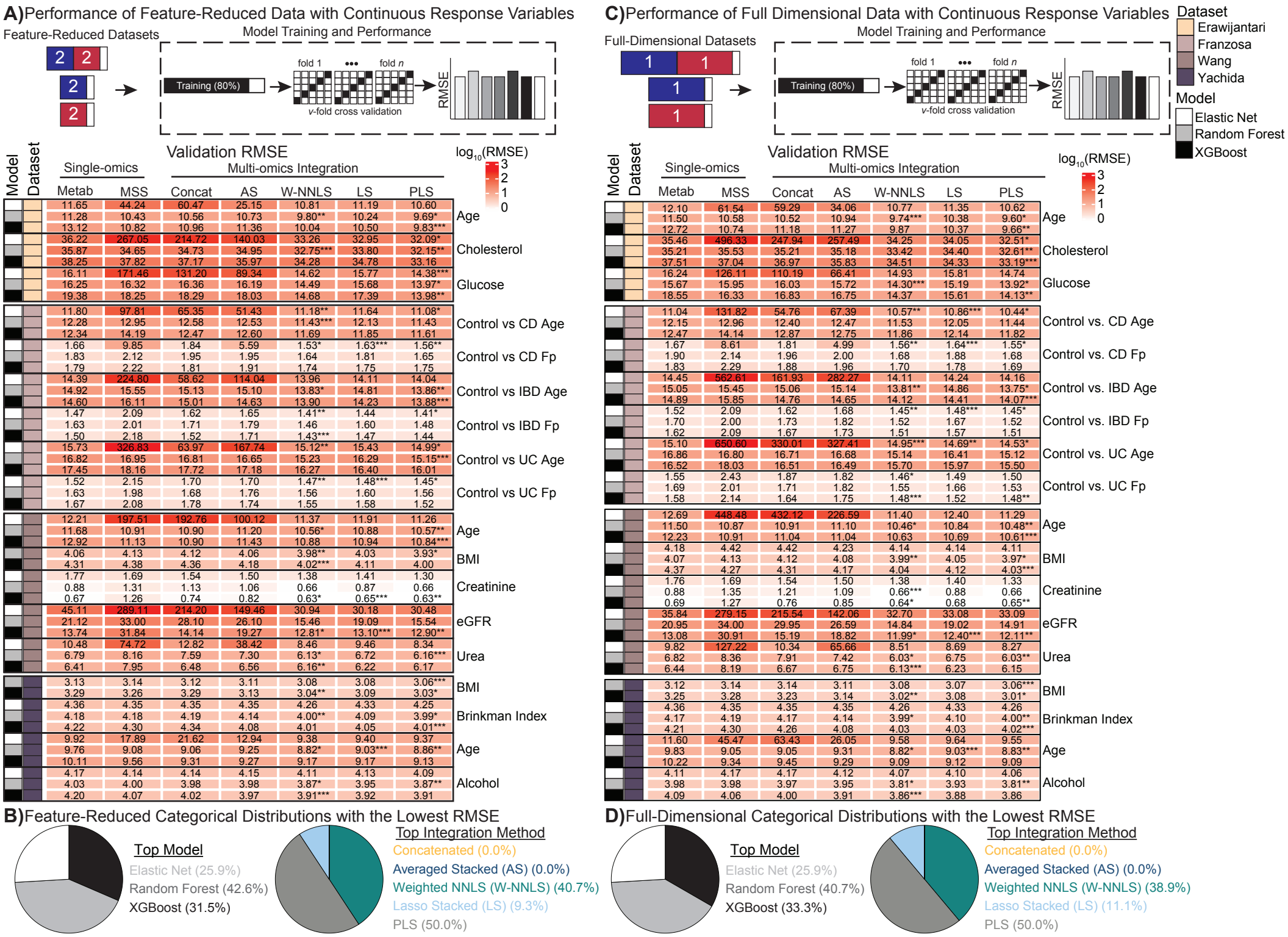
A) Performance of Feature-Reduced Data with Continuous Response Variables
Feature-Reduced Datasets
Model Training and Performance
Training (80%)
fold 1
fold n
v-fold cross validation
RMSE
Validation RMSE
Model
Dataset
Single-omics
Multi-omics Integration
Metab
MSS
Concat
AS
W-NNLS
LS
PLS
log10(RMSE)
3
2
1
0
Age
Cholesterol
Glucose
Control vs CD Age
Control vs CD Fp
Control vs IBD Age
Control vs IBD Fp
Control vs UC Age
Control vs UC Fp
Age
BMI
Creatinine
eGFR
Urea
BMI
Brinkman Index
Age
Alcohol
B) Feature-Reduced Categorical Distributions with the Lowest RMSE
Top Model
Elastic Net (25.9%)
Random Forest (42.6%)
XGBoost (31.5%)
Top Integration Method
Concatenated (0.0%)
Averaged Stacked (AS) (0.0%)
Weighted NNLS (W-NNLS) (40.7%)
Lasso Stacked (LS) (9.3%)
PLS (50.0%)
C) Performance of Full Dimensional Data with Continuous Response Variables
Full-Dimensional Datasets
Model Training and Performance
Training (80%)
fold 1
fold n
v-fold cross validation
RMSE
Validation RMSE
Model
Dataset
Single-omics
Multi-omics Integration
Metab
MSS
Concat
AS
W-NNLS
LS
PLS
log10(RMSE)
3
2
1
0
Age
Cholesterol
Glucose
Control vs. CD Age
Control vs. CD Fp
Control vs. IBD Age
Control vs. IBD Fp
Control vs. UC Age
Control vs. UC Fp
Age
BMI
Creatinine
eGFR
Urea
BMI
Brinkman Index
Age
Alcohol
D) Full-Dimensional Categorical Distributions with the Lowest RMSE
Top Model
Elastic Net (25.9%)
Random Forest (40.7%)
XGBoost (33.3%)
Top Integration Method
Concatenated (0.0%)
Averaged Stacked (AS) (0.0%)
Weighted NNLS (W-NNLS) (38.9%)
Lasso Stacked (LS) (11.1%)
PLS (50.0%)
Dataset
Erawijantari
Franzosa
Wang
Yachida
Model
Elastic Net
Random Forest
XGBoost

Supplemental Figure 1. **Validation Performance Metrics Across Continuous Feature-Reduced and Full-Dimensional Datasets.** Validation performance for feature-reduced matched microbiome and metabolomics datasets with continuous response variables are represented by **A)**. The top performing machine learning models and top integration methods for each of the feature-reduced datasets are represented as pie charts in **B)**. Validation performance for full-dimensional matched microbiome and metabolomics datasets with continuous response variables are represented by **C)**. The top performing machine learning models and top integration methods for each of the full-dimensional datasets are represented as pie charts in **D)**. Performance calculated using RMSE Mean. Actual RMSE values are shown in each cell of the heatmap with $\log_{10}$ scaling for the coloring. Response variables used for each model are shown on the right of each heatmap. The top performing models per response variable are represented by '*', where '*' is the best performing model, '**' is the second-best performing model and '***' is the third-best performing model. The proportions are calculated using the top three best performing models (*, **, ***) per response variable. 'T' represents ties in performance; response variables with majority 'T' were not used for pie chart calculations. Individual omics (Metabolomics and MSS) were not represented in the pie charts. '>' or 'T' represents increased or tied performance of an individual omics to one of the top performing integration models ('*', '**', and '***').

A) Performance of Feature-Reduced Data with Binary Response Variables

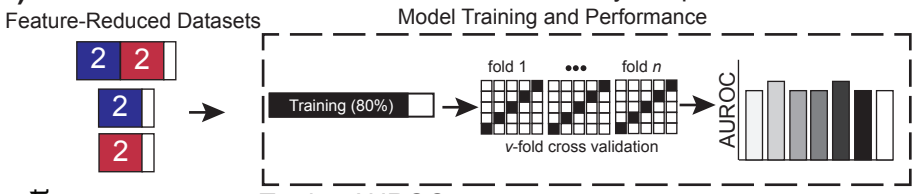

Testing AUROC

Model	Dataset	Single-omics: Metab	Single-omics: MSS	Multi-omics Integration: Concat	AS	W-NNLS	LS	PLS
	No Alcohol vs. Alcohol	0.54	0.60	0.60	0.58	0.55	0.59	0.58
		0.56	0.74>*	0.71*	0.66	0.62	0.68**	0.64
		0.59	0.67>***	0.64	0.67***	0.52	0.66	0.65
	Female vs. Male	0.58	0.75>*	0.73*	0.52	0.72**	0.63***	0.60
		0.51	0.59	0.61	0.54	0.56	0.54	0.57
	Control vs. Gastrectomy	1.00T	0.83	0.99	1.00T	1.00T	1.00T	1.00T
		1.00T	0.91	0.96	1.00T	1.00T	1.00T	1.00T
		1.00T	0.89	1.00T	0.99	1.00T	0.99	1.00T
	Control vs. Chrohn's Disease	0.97>***	0.92	0.96	0.97	0.97	0.97	0.97
		0.97	0.97	0.97	0.97	0.97*	0.97**	0.97***
		0.97	0.97	0.97	0.97	0.97	0.97	0.97
	Control vs. IBD	0.94	0.84	0.91	0.94	0.95	0.94	0.92
		0.94	0.91	0.95	0.95***	0.95	0.94	0.94
		0.93	0.93	0.95	0.96*	0.96**	0.95	0.95
	Control vs. Ulcerative Colitis	0.93	0.83	0.95	0.93	0.94	0.94	0.91
		0.97	0.96	0.97	0.97	0.98*	0.98***	0.98**
		0.95	0.95	0.96	0.97	0.97	0.96	0.95
	Female vs. Male	0.60>***	0.55	0.54	0.63*	0.57	0.57	0.57
		0.55	0.56	0.56	0.60**	0.57	0.58***	0.57
	Control vs. Kidney Failure	1.00T	0.95	0.98	1.00T	1.00T	1.00T	1.00T
		1.00T	0.98	1.00T	1.00T	1.00T	1.00T	1.00T
		1.00T	0.98	1.00T	1.00T	1.00T	1.00T	1.00T
	Female vs. Male	0.69	0.64	0.68	0.70	0.72	0.69	0.69
		0.75	0.64	0.73	0.75***	0.76*	0.75	0.76**
		0.71	0.67	0.75	0.74	0.74	0.73	0.74
	Control vs. MP & CRC	0.74	0.65	0.66	0.71	0.73	0.73	0.73
		0.73	0.80>***	0.80**	0.80	0.77	0.80***	0.81*
		0.70	0.74	0.76	0.76	0.77	0.76	0.74
	Control vs. MP & Stage 0 CRC	0.69	0.59	0.61	0.71	0.64	0.69	0.69
		0.74	0.83>***	0.83***	0.86*	0.77	0.84**	0.82
		0.65	0.75	0.72	0.75	0.65	0.74	0.72
	Control vs. Stage 1 & 2 CRC	0.76	0.72	0.76	0.78	0.78	0.77	0.77
		0.65	0.86>***	0.87*	0.81	0.86**	0.85***	0.83
		0.64	0.83	0.81	0.75	0.81	0.78	0.77
	Control vs. Stage 3 & 4 CRC	0.82	0.81	0.83	0.87	0.86	0.85	0.83
		0.86	0.94>***	0.94**	0.93	0.94*	0.93	0.93***
		0.79	0.87	0.86	0.86	0.84	0.87	0.87

C) Performance of Full-Dimensional Data with Binary Response Variables

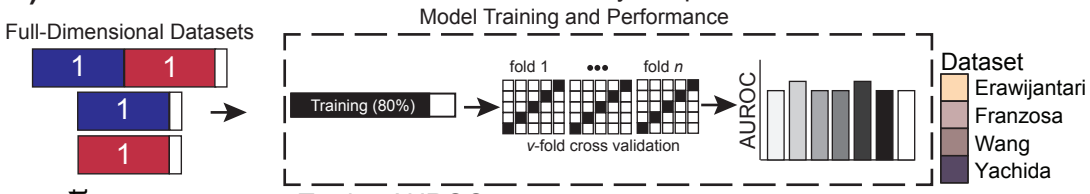

Testing AUROC

Model: Elastic Net, Random Forest, XGBoost

AUROC: 1, 0.5, 0

Model	Dataset	Single-omics: Metab	Single-omics: MSS	Multi-omics Integration: Concat	AS	W-NNLS	LS	PLS
	No Alcohol vs. Alcohol	0.53	0.59	0.55	0.56	0.54	0.54	0.53
		0.61	0.73>*	0.71**	0.71*	0.62	0.63	0.68***
		0.55	0.66	0.67	0.63	0.62	0.61	0.60
	Female vs. Male	0.55	0.55	0.58	0.56	0.58	0.55	0.56
		0.70>*	0.58	0.59	0.63***	0.59	0.67**	0.68*
		0.57	0.58	0.56	0.56	0.53	0.57	0.55
	Control vs. Gastrectomy	1.00T	0.75	0.99	0.98	1.00T	1.00T	1.00T
		1.00T	0.87	0.94	1.00T	1.00T	1.00T	1.00T
		1.00T	0.87	0.99	1.00T	1.00T	1.00T	1.00T
	Control vs. Chrohn's Disease	0.98>*	0.94	0.96	0.97	0.98**	0.97	0.98*
		0.97	0.97>***	0.97	0.97	0.97	0.97***	0.97
		0.97	0.97	0.97	0.97	0.97	0.97	0.97
	Control vs. IBD	0.94	0.85	0.92	0.94	0.95	0.94	0.93
		0.93	0.91	0.94	0.94	0.94	0.93	0.93
		0.93	0.94	0.95	0.96**	0.96*	0.95***	0.95
	Control vs. Ulcerative Colitis	0.93	0.75	0.95	0.92	0.92	0.93	0.92
		0.95	0.96	0.97	0.97	0.98*T	0.96	0.96
		0.94	0.96	0.95	0.97***	0.98*T	0.96	0.95
	Female vs. Male	0.59>*	0.53	0.52	0.58*	0.56	0.55	0.56
		0.56	0.56	0.54	0.57**	0.57	0.57***	0.56
	Control vs. Kidney Failure	1.00T	0.93	0.98	1.00T	1.00T	1.00T	1.00T
		1.00T	0.98	1.00T	1.00T	1.00T	1.00T	1.00T
		1.00T	0.97	1.00T	1.00T	1.00T	1.00T	1.00T
	Female vs. Male	0.72	0.66	0.70	0.73	0.75	0.72	0.72
		0.81>**	0.68	0.72	0.78	0.81*	0.80**	0.80***
		0.78	0.68	0.76	0.77	0.79	0.78	0.78
	Control vs. MP & CRC	0.71	0.56	0.55	0.63	0.69	0.69	0.67
		0.71	0.72	0.74***	0.75*	0.72	0.73	0.75**
		0.63	0.69	0.69	0.69	0.70	0.69	0.68
	Control vs. MP and Stage 0 CRC	0.69	0.75>***	0.76**	0.76*	0.57	0.74***	0.69
		0.63	0.60	0.62	0.64	0.56	0.62	0.61
	Control vs. Stage 1 & 2 CRC	0.58	0.72>**	0.72*	0.68**	0.66***	0.63	0.64
		0.61	0.65	0.63	0.64	0.59	0.65	0.62
	Control vs. Stage 3 & 4 CRC	0.72	0.66	0.69	0.75	0.71	0.72	0.73
		0.89	0.89	0.91**	0.94*	0.85	0.90***	0.89
		0.85	0.80	0.82	0.88	0.86	0.83	0.82

B) Feature-Reduced Categorical Distributions with the Lowest AUROC

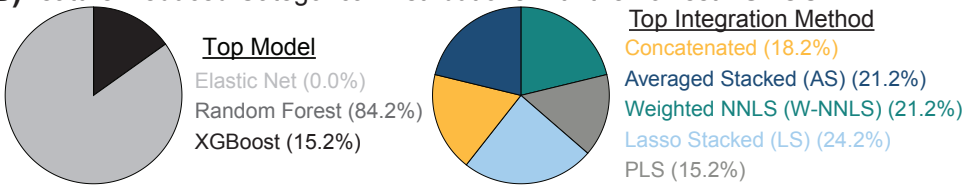

D) Full-Dimensional Categorical Distributions with the Lowest AUROC

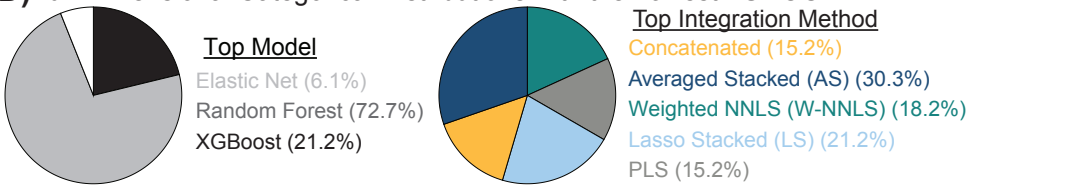

Figure 3. Test Performance Metrics Across Binary Feature-Reduced and Full-Dimensional Datasets. Testing performance for feature-reduced matched microbiome and metabolomics datasets with binary response variables are represented by **A)**. The top performing machine learning models and top integration methods for each of the feature-reduced datasets are represented as pie charts in **B)**. Testing performance for full-dimensional matched microbiome and metabolomics datasets with binary response variables are represented by **C)**. The top performing machine learning models and top integration methods for each of the full-dimensional datasets are represented as pie charts in **D)**. Performance is calculated using AUROC mean, which are shown in the heatmap. Response variables used for each model are shown on the right of each heatmap. The top performing models per response variable are represented by '*', where '*' is the best performing model, '**' is the second-best performing model and '***' is the third-best performing model. The proportions are calculated using the top three best performing models (*, **, ***) per response variable. 'T' represents ties in performance; response variables with majority 'T' were not used for pie chart calculations. Individual omics (Metabolomics and MSS) were not represented in the pie charts. '>' or 'T' represents increased or tied performance of an individual omics to one of the top performing integration models ('*', '**', and '***').

A) Performance of Feature-Reduced Data with Binary Response Variables

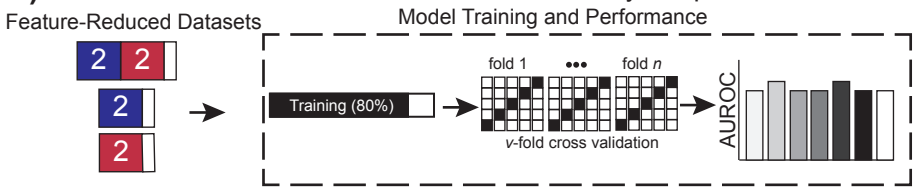

Validation AUROC

Model	Dataset	Metab (Single-omics)	MSS (Single-omics)	Concat (Multi-omics Integration)	AS (Multi-omics Integration)	W-NNLS (Multi-omics Integration)	LS (Multi-omics Integration)	PLS (Multi-omics Integration)	
Elastic Net		0.59	0.60	0.62	0.60	0.59	0.59	0.65	No Alcohol vs. Alcohol
Random Forest		0.63	0.64	0.63	0.67***	0.60	0.70*	0.69**	
XGBoost		0.54	0.57	0.58	0.60	0.53	0.60	0.63	
Random Forest		0.72	0.71	0.69	0.76***	0.75	0.79**	0.80*	Female vs. Male
XGBoost		0.64	0.62	0.68	0.70	0.65	0.71	0.72	
Elastic Net		0.97	0.76	0.87	0.93	0.97	0.96	0.97	Control vs. Gastrectomy
Random Forest		0.95	0.90	0.93	0.98**	0.98*	0.98	0.98***	
XGBoost		0.92	0.87	0.94	0.96	0.98	0.96	0.97	
Elastic Net		0.94	0.87	0.93	0.93	0.94	0.94	0.94	Control vs. Chrohn's Disease
Random Forest		0.93	0.94	0.94	0.94	0.94	0.94	0.94	
XGBoost		0.94	0.93	0.93	0.94	0.95***	0.95**	0.95**	
Elastic Net		0.95	0.83	0.90	0.94	0.95***	0.95**	0.95*	Control vs. IBD
Random Forest		0.91	0.88	0.91	0.91	0.91	0.92	0.91	
XGBoost		0.92	0.88	0.92	0.92	0.93	0.93	0.92	
Elastic Net		0.96	0.75	0.93	0.93	0.96***	0.96	0.96	Control vs. Ulcerative Colitis
Random Forest		0.94	0.85	0.94	0.94	0.94	0.95	0.94	
XGBoost		0.96	0.85	0.95	0.95	0.96*	0.96	0.96**	
Random Forest		0.57	0.63	0.62	0.60	0.61	0.64***	0.65*	Female vs. Male
XGBoost		0.60	0.62	0.60	0.64	0.63	0.64**	0.63	
Elastic Net		1.00[T]	0.89	0.97	1.00[T]	1.00[T]	1.00[T]	1.00[T]	Control vs. Kidney Failure
Random Forest		1.00[T]	0.90	0.98	1.00[T]	1.00[T]	1.00[T]	1.00[T]	
XGBoost		1.00[T]	0.92	1.00[T]	1.00[T]	1.00[T]	1.00[T]	1.00[T]	
Elastic Net		0.70	0.71	0.73	0.75	0.76	0.76	0.76	Female vs. Male
Random Forest		0.77	0.64	0.74	0.77	0.79**	0.78	0.79*	
XGBoost		0.77	0.64	0.76	0.77	0.79	0.79	0.79***	
Elastic Net		0.68	0.65	0.69	0.68	0.72	0.73	0.72	Control vs. MP & CRC
Random Forest		0.70	0.77	0.77	0.78***	0.78	0.79**	0.79*	
XGBoost		0.64	0.75	0.74	0.73	0.76	0.75	0.76	
Elastic Net		0.68	0.51	0.54	0.66	0.66	0.67	0.68***	Control vs. MP & Stage 0 CRC
Random Forest		0.56	0.67	0.65	0.67	0.67	0.68**	0.67	
XGBoost		0.59	0.67	0.65	0.65	0.65	0.68	0.69*	
Elastic Net		0.80	0.74	0.78	0.80	0.83***	0.83**	0.83	Control vs. Stage 1 & 2 CRC
Random Forest		0.73	0.80	0.80	0.81	0.83*	0.82	0.82	
XGBoost		0.70	0.77	0.77	0.78	0.78	0.79	0.79	
Elastic Net		0.77	0.69	0.68	0.76	0.78	0.79	0.79	Control vs. Stage 3 & 4 CRC
Random Forest		0.69	0.82	0.83	0.80	0.83**	0.84*	0.83	
XGBoost		0.64	0.83	0.83	0.80	0.81	0.82	0.83***	

B) Feature-Reduced Categorical Distributions with the Lowest AUROC

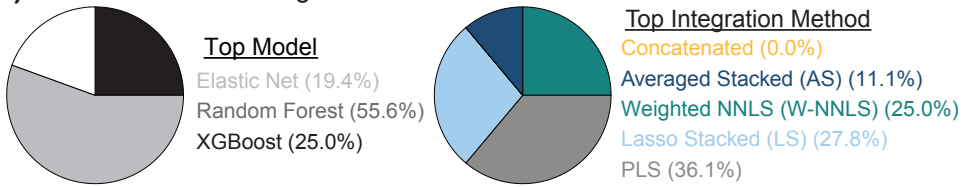

C) Performance of Full-Dimensional Data with Binary Response Variables

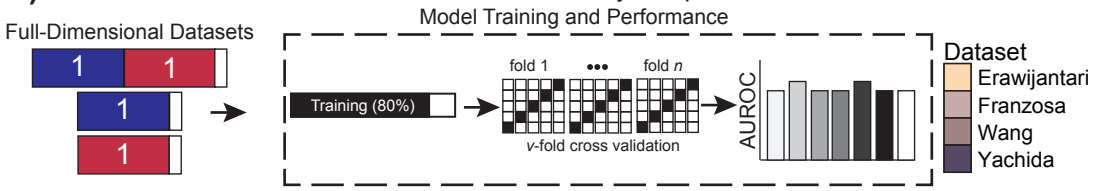

Validation AUROC

Model: Elastic Net, Random Forest, XGBoost

AUROC: 1, 0.5, 0

Model	Dataset	Metab (Single-omics)	MSS (Single-omics)	Concat (Multi-omics Integration)	AS (Multi-omics Integration)	W-NNLS (Multi-omics Integration)	LS (Multi-omics Integration)	PLS (Multi-omics Integration)	
Elastic Net		0.66	0.60	0.63	0.61	0.63	0.67	0.69	No Alcohol vs. Alcohol
Random Forest		0.64	0.60	0.60	0.61	0.67	0.67	0.70*[T]	
XGBoost		0.68	0.60	0.59	0.66	0.66	0.69***	0.70*[T]	
Elastic Net		0.73[T]***	0.54	0.69	0.74**	0.73	0.73***	0.75*	Female vs. Male
Random Forest		0.68	0.61	0.64	0.66	0.65	0.68	0.70	
XGBoost		0.65	0.62	0.60	0.64	0.59	0.66	0.68	
Elastic Net		0.97	0.68	0.88	0.90	0.98*	0.97**	0.97***	Control vs. Gastrectomy
Random Forest		0.93	0.87	0.92	0.96	0.97	0.95	0.97	
XGBoost		0.94	0.84	0.91	0.94	0.96	0.96	0.96	
Elastic Net		0.94	0.89	0.93	0.93	0.94**	0.94***	0.94	Control vs. Chrohn's Disease
Random Forest		0.93	0.93	0.94	0.94	0.94	0.94	0.94	
XGBoost		0.94	0.93	0.94	0.94	0.95*	0.94	0.94	
Elastic Net		0.93***	0.84	0.90	0.92	0.93**	0.94*	0.93***	Control vs. IBD
Random Forest		0.91	0.88	0.91	0.91	0.91	0.91	0.91	
XGBoost		0.91	0.87	0.91	0.91	0.92	0.92	0.91	
Elastic Net		0.96	0.77	0.94	0.94	0.97*	0.96***	0.96**	Control vs. Ulcerative Colitis
Random Forest		0.92	0.84	0.93	0.93	0.93	0.93	0.93	
XGBoost		0.94	0.84	0.93	0.94	0.95	0.95	0.95	
Random Forest		0.57	0.59	0.59	0.59	0.61	0.62	0.63	Female vs. Male
XGBoost		0.62	0.61	0.59	0.65***	0.65	0.67*	0.67**	
Elastic Net		0.99	0.87	0.96	0.99	1.00[T]	0.99	0.99	Control vs. Kidney Failure
Random Forest		1.00[T]	0.89	0.97	1.00[T]	1.00[T]	1.00[T]	1.00[T]	
XGBoost		1.00[T]	0.91	1.00[T]	1.00[T]	1.00[T]	1.00[T]	1.00[T]	
Elastic Net		0.69	0.67	0.70	0.73	0.75	0.75	0.75	Female vs. Male
Random Forest		0.80	0.66	0.72	0.78	0.81**	0.80	0.81*	
XGBoost		0.79	0.68	0.79	0.79	0.81***	0.80	0.81	
Elastic Net		0.65	0.61	0.60	0.63	0.69	0.69	0.70	Control vs. MP and CRC
Random Forest		0.71	0.70	0.71	0.74	0.75***	0.75**	0.76*	
XGBoost		0.69	0.70	0.72	0.72	0.74	0.74	0.74	
Random Forest		0.55	0.58	0.56	0.56	0.55	0.58	0.61**	Control vs. MP & Stage 0 CRC
XGBoost		0.58	0.58	0.61***	0.58	0.56	0.60	0.62*	
Random Forest		0.64	0.60	0.61	0.64	0.64	0.67	0.67	Control vs. Stage 1 & 2 CRC
XGBoost		0.66	0.65	0.62	0.67***	0.62	0.69**	0.69*	
Random Forest		0.70	0.59	0.58	0.70	0.70	0.70	0.72	Control vs. Stage 3 & 4 CRC
XGBoost		0.69	0.71	0.71	0.73	0.74	0.75	0.77	
XGBoost		0.64	0.78	0.76	0.76	0.79***	0.79**	0.80*	

D) Full-Dimensional Categorical Distributions with the Lowest AUROC

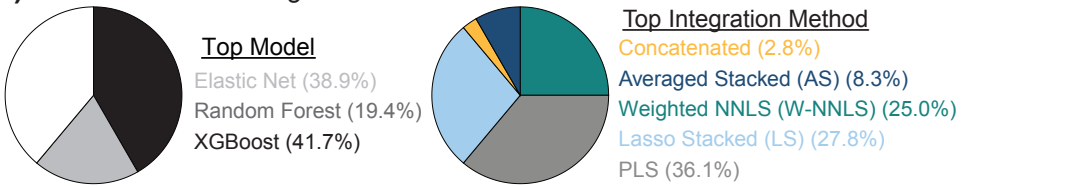

Supplemental Figure 2. Validation Performance Metrics Across Binary Feature-Reduced and Full-Dimensional Datasets. Validation performance for feature-reduced matched microbiome and metabolomics datasets with binary response variables are represented by **A)**. The top performing machine learning models and top integration methods for each of the feature-reduced datasets are represented as pie charts in **B)**. Testing performance for full-dimensional matched microbiome and metabolomics datasets with binary response variables are represented by **C)**. The top performing machine learning models and top integration methods for each of the full-dimensional datasets are represented as pie charts in **D)**. Performance is calculated using AUROC mean, which are shown in the heatmap. Response variables used for each model are shown on the right of each heatmap. The top performing models per response variable are represented by '*', where '*' is the best performing model, '**' is the second-best performing model and '***' is the third-best performing model. The proportions are calculated using the top three best performing models (*, **, ***) per response variable. 'T' represents ties in performance; response variables with majority 'T' were not used for pie chart calculations. Individual omics (Metabolomics and MSS) were not represented in the pie charts. '>' or 'T' represents increased or tied performance of an individual omics to one of the top performing integration models ('*', '**', and '***').

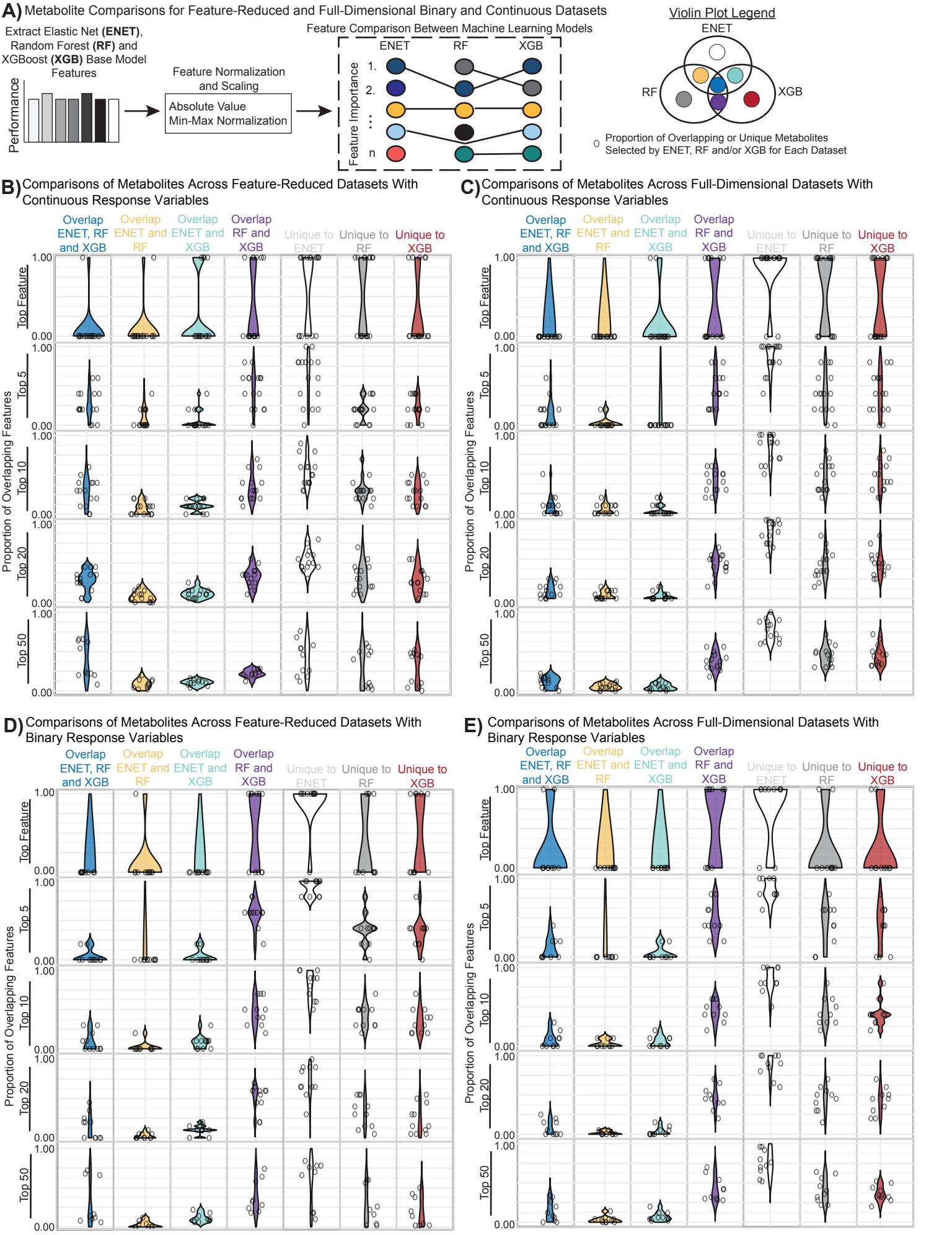
A) Metabolite Comparisons for Feature-Reduced and Full-Dimensional Binary and Continuous Datasets
Extract Elastic Net (ENET), Random Forest (RF) and XGBoost (XGB) Base Model Features
Performance
Feature Normalization and Scaling
Absolute Value
Min-Max Normalization
Feature Comparison Between Machine Learning Models
ENET
RF
XGB
Feature Importance
1.
2.
n
Violin Plot Legend
ENET
RF
XGB
Proportion of Overlapping or Unique Metabolites Selected by ENET, RF and/or XGB for Each Dataset
B) Comparisons of Metabolites Across Feature-Reduced Datasets With Continuous Response Variables
C) Comparisons of Metabolites Across Full-Dimensional Datasets With Continuous Response Variables
D) Comparisons of Metabolites Across Feature-Reduced Datasets With Binary Response Variables
E) Comparisons of Metabolites Across Full-Dimensional Datasets With Binary Response Variables
Overlap ENET, RF and XGB
Overlap ENET and RF
Overlap ENET and XGB
Overlap RF and XGB
Unique to ENET
Unique to RF
Unique to XGB
Proportion of Overlapping Features
Top Feature
Top 5
Top 10
Top 20
Top 50
1.00
0.00

Figure 4. Metabolite Feature Selection Comparisons across Elastic Net, Random Forest and XGBoost. The pipeline for extracting feature importance metrics and performing comparisons are represented in **A)**. Feature Importance values for Elastic Net (ENET), Random Forest (RF) and XGBoost (XGB) were extracted for each cross-validation step. The absolute value was taken for each value and min-max normalization was performed. The overall average for each feature was then used as the metric for feature importance. See **Methods** for more details. Comparisons for the metabolites selected across feature-reduced datasets with continuous response variables are represented by **B)**. Comparisons for the metabolites selected across full-dimensional datasets with continuous response variables are represented by **C)**. Comparisons for the metabolites selected across feature-reduced datasets with binary response variables are represented by **D)**. Comparisons for the metabolites selected across full-dimensional datasets with binary response variables are represented by **E)**. For each analysis, top features for ENET, RF and XGB were binned into 5 levels – top feature (i.e., features with highest feature importance values), top 5 features, top 10 features, top 20 features and top 50 features. For each bin, comparisons for the features selected between ENET, RF and XGB were performed to identify joint and unique features. The distribution of dataset proportions for overlapping and unique features are represented by violin plots for panels **B-E**.

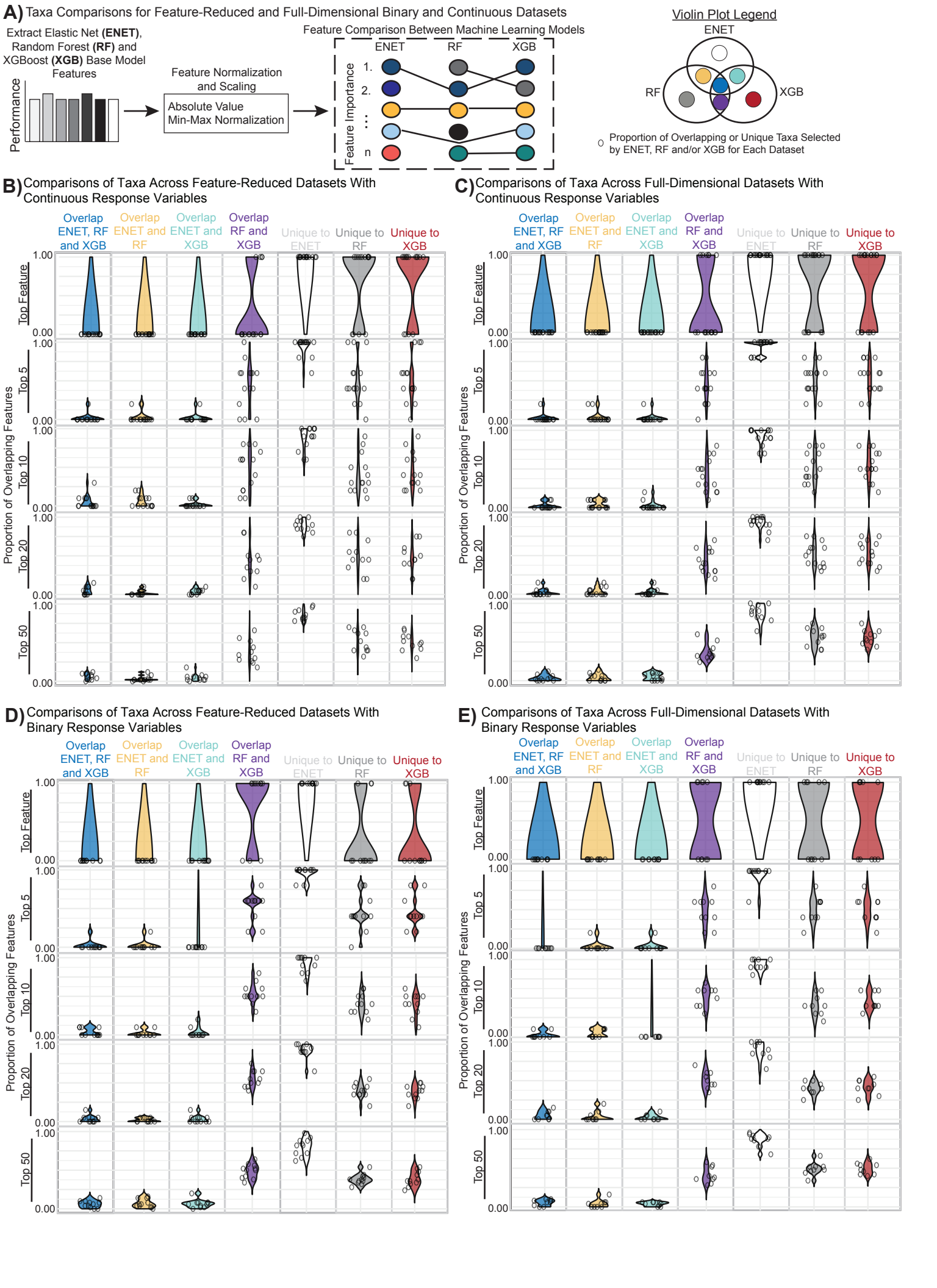
A) Taxa Comparisons for Feature-Reduced and Full-Dimensional Binary and Continuous Datasets
Extract Elastic Net (ENET), Random Forest (RF) and XGBoost (XGB) Base Model Features
Performance
Feature Normalization and Scaling
Absolute Value
Min-Max Normalization
Feature Comparison Between Machine Learning Models
ENET
RF
XGB
Feature Importance
1.
2.
n
Violin Plot Legend
ENET
RF
XGB
Proportion of Overlapping or Unique Taxa Selected by ENET, RF and/or XGB for Each Dataset
B) Comparisons of Taxa Across Feature-Reduced Datasets With Continuous Response Variables
C) Comparisons of Taxa Across Full-Dimensional Datasets With Continuous Response Variables
D) Comparisons of Taxa Across Feature-Reduced Datasets With Binary Response Variables
E) Comparisons of Taxa Across Full-Dimensional Datasets With Binary Response Variables
Overlap ENET, RF and XGB
Overlap ENET and RF
Overlap ENET and XGB
Overlap RF and XGB
Unique to ENET
Unique to RF
Unique to XGB
Proportion of Overlapping Features
Top Feature
Top 5
Top 10
Top 20
Top 50
1.00
0.00

Figure 5. Taxa Feature Selection Comparisons across Elastic Net, Random Forest and XGBoost. The pipeline for extracting feature importance metrics and performing comparisons are represented in **A)**. Feature Importance values for Elastic Net (ENET), Random Forest (RF) and XGBoost (XGB) were extracted for each cross-validation step. The absolute value was taken for each value and min-max normalization was performed. The overall average for each feature was then used as the metric for feature importance. See **Methods** for more details. Comparisons for the taxa selected across feature-reduced datasets with continuous response variables are represented by **B)**. Comparisons for the taxa selected across full-dimensional datasets with continuous response variables are represented by **C)**. Comparisons for the taxa selected across feature-reduced datasets with binary response variables are represented by **D)**. Comparisons for the taxa selected across full-dimensional datasets with binary response variables are represented by **E)**. For each analysis, top features for ENET, RF and XGB were binned into 5 levels – top feature (i.e., features with highest feature importance values), top 5 features, top 10 features, top 20 features and top 50 features. For each bin, comparisons for the features selected between ENET, RF and XGB were performed to identify joint and unique features. The distribution of dataset proportions for overlapping and unique features are represented by violin plots for panels **B-E**.

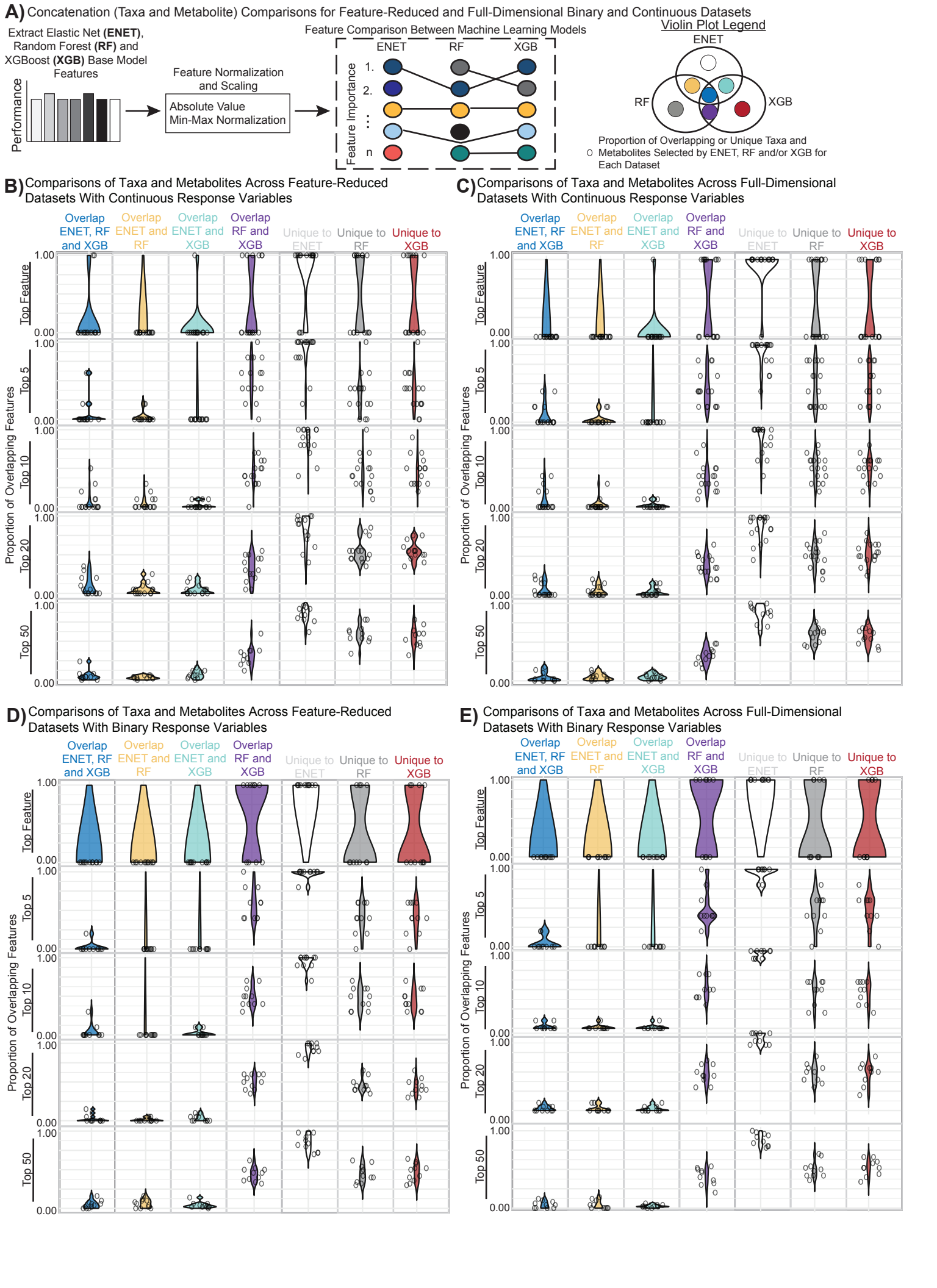
A) Concatenation (Taxa and Metabolite) Comparisons for Feature-Reduced and Full-Dimensional Binary and Continuous Datasets
Extract Elastic Net (ENET), Random Forest (RF) and XGBoost (XGB) Base Model Features
Performance
Feature Normalization and Scaling
Absolute Value
Min-Max Normalization
Feature Comparison Between Machine Learning Models
ENET
RF
XGB
Feature Importance
1.
2.
n
Violin Plot Legend
ENET
RF
XGB
Proportion of Overlapping or Unique Taxa and Metabolites Selected by ENET, RF and/or XGB for Each Dataset
B) Comparisons of Taxa and Metabolites Across Feature-Reduced Datasets With Continuous Response Variables
C) Comparisons of Taxa and Metabolites Across Full-Dimensional Datasets With Continuous Response Variables
D) Comparisons of Taxa and Metabolites Across Feature-Reduced Datasets With Binary Response Variables
E) Comparisons of Taxa and Metabolites Across Full-Dimensional Datasets With Binary Response Variables
Overlap ENET, RF and XGB
Overlap ENET and RF
Overlap ENET and XGB
Overlap RF and XGB
Unique to ENET
Unique to RF
Unique to XGB
Proportion of Overlapping Features
Top Feature
Top 5
Top 10
Top 20
Top 50
1.00
0.00

Figure 6. Concatenation Feature Selection Comparisons across Elastic Net, Random Forest and XGBoost. The pipeline for extracting feature importance metrics and performing comparisons are represented in **A)**. Feature Importance values for Elastic Net (ENET), Random Forest (RF) and XGBoost (XGB) were extracted for each cross-validation step. The absolute value was taken for each value and min-max normalization was performed. The overall average for each feature was then used as the metric for feature importance. See **Methods** for more details. Comparisons for the metabolites and taxa selected across feature-reduced datasets with continuous response variables are represented by **B)**. Comparisons for the metabolites and taxa selected across full-dimensional datasets with continuous response variables are represented by **C)**. Comparisons for the metabolites and taxa selected across feature-reduced datasets with binary response variables are represented by **D)**. Comparisons for the metabolites and taxa selected across full-dimensional datasets with binary response variables are represented by **E)**. For each analysis, top features for ENET, RF and XGB were binned into 5 levels – top feature (i.e., features with highest feature importance values), top 5 features, top 10 features, top 20 features and top 50 features. For each bin, comparisons for the features selected between ENET, RF and XGB were performed to identify joint and unique features. The distribution of dataset proportions for overlapping and unique features are represented by violin plots for panels **B-E**.

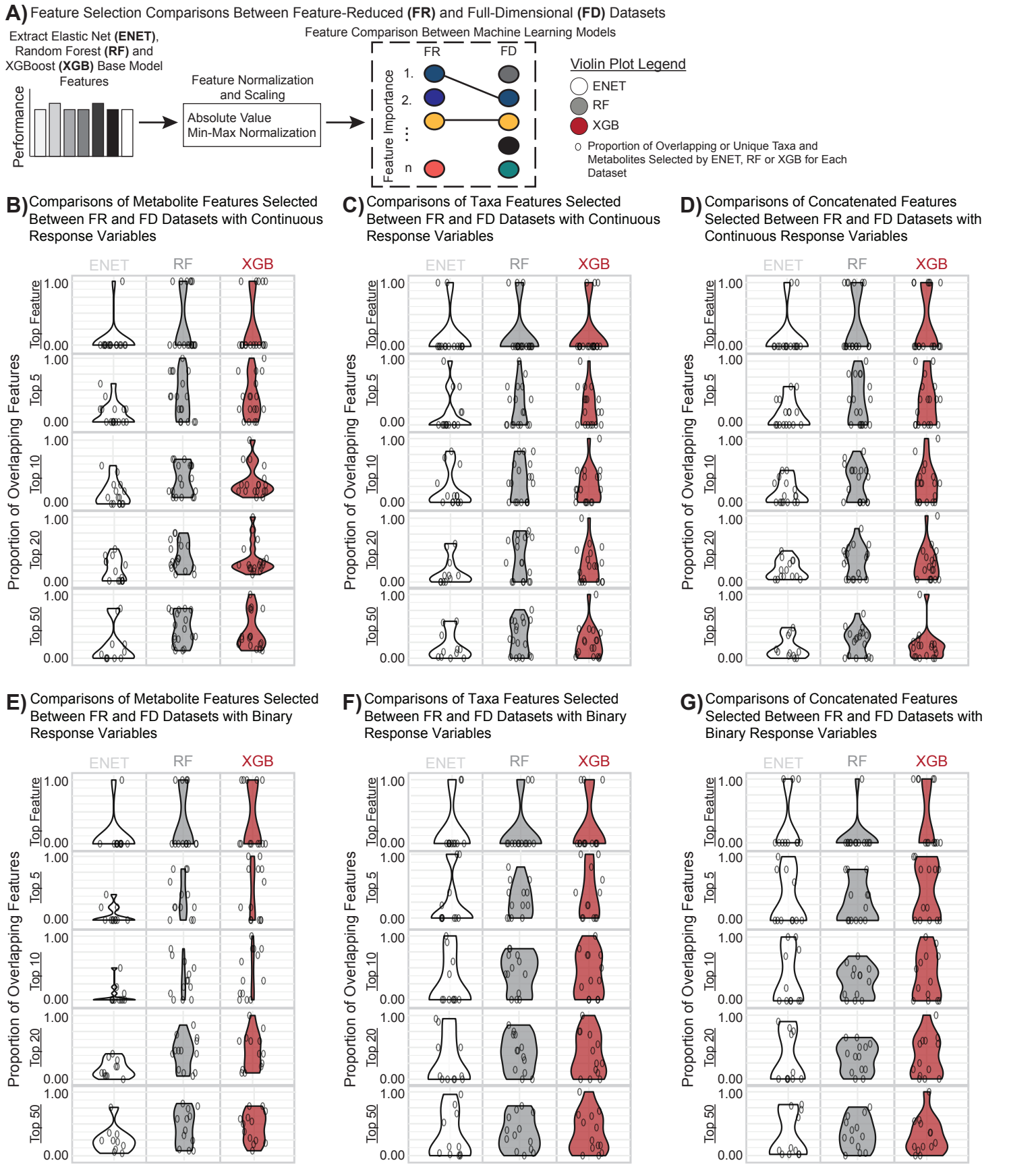
A) Feature Selection Comparisons Between Feature-Reduced (FR) and Full-Dimensional (FD) Datasets
Extract Elastic Net (ENET), Random Forest (RF) and XGBoost (XGB) Base Model Features
Performance
Feature Normalization and Scaling
Absolute Value
Min-Max Normalization
Feature Comparison Between Machine Learning Models
FR
FD
Feature Importance
1.
2.
n
Violin Plot Legend
ENET
RF
XGB
Proportion of Overlapping or Unique Taxa and Metabolites Selected by ENET, RF or XGB for Each Dataset
B) Comparisons of Metabolite Features Selected Between FR and FD Datasets with Continuous Response Variables
C) Comparisons of Taxa Features Selected Between FR and FD Datasets with Continuous Response Variables
D) Comparisons of Concatenated Features Selected Between FR and FD Datasets with Continuous Response Variables
E) Comparisons of Metabolite Features Selected Between FR and FD Datasets with Binary Response Variables
F) Comparisons of Taxa Features Selected Between FR and FD Datasets with Binary Response Variables
G) Comparisons of Concatenated Features Selected Between FR and FD Datasets with Binary Response Variables
ENET
RF
XGB
Proportion of Overlapping Features
Top Feature
Top 5
Top 10
Top 20
Top 50
1.00
0.00

Figure 7. Feature Selection Comparisons Between Featured-Reduced (FR) and Full-Dimensional (FD) Datasets Across Elastic Net (ENET), Random Forest (RF) and XGBoost (XGB) Models. The pipeline for extracting feature importance metrics and performing comparisons are represented in **A)**. Feature Importance values for ENET, RF and XGB were extracted for each cross-validation step. The absolute value was taken for each value and min-max normalization was performed. The overall average for each feature was then used as the metric for feature importance. See **Methods** for more details. Comparisons for the metabolites selected by feature-reduced and full-dimensional datasets with continuous response variables are represented by **B)**. Comparisons for the taxa selected by feature-reduced and full-dimensional datasets with continuous response variables are represented by **C)**. Comparisons for the taxa and metabolites selected by feature-reduced and full-dimensional datasets with continuous response variables are represented by **D)**. Comparisons for the metabolites selected by feature-reduced and full-dimensional datasets with binary response variables are represented by **E)**. Comparisons for the taxa selected by feature-reduced and full-dimensional datasets with binary response variables are represented by **F)**. Comparisons for the taxa and metabolites selected by feature-reduced and full-dimensional datasets with continuous response variables are represented by **G)**. For each analysis, top features for ENET, RF and XGB were binned into 5 levels – top feature (i.e., features with highest feature importance values), top 5 features, top 10 features, top 20 features and top 50 features. For each bin, comparisons for the features selected by feature-reduced and full-dimensional datasets for ENET, RF and XGB were performed to identify joint and unique features. The distribution of dataset proportions for overlapping and unique features are represented by violin plots for panels **B-G**.

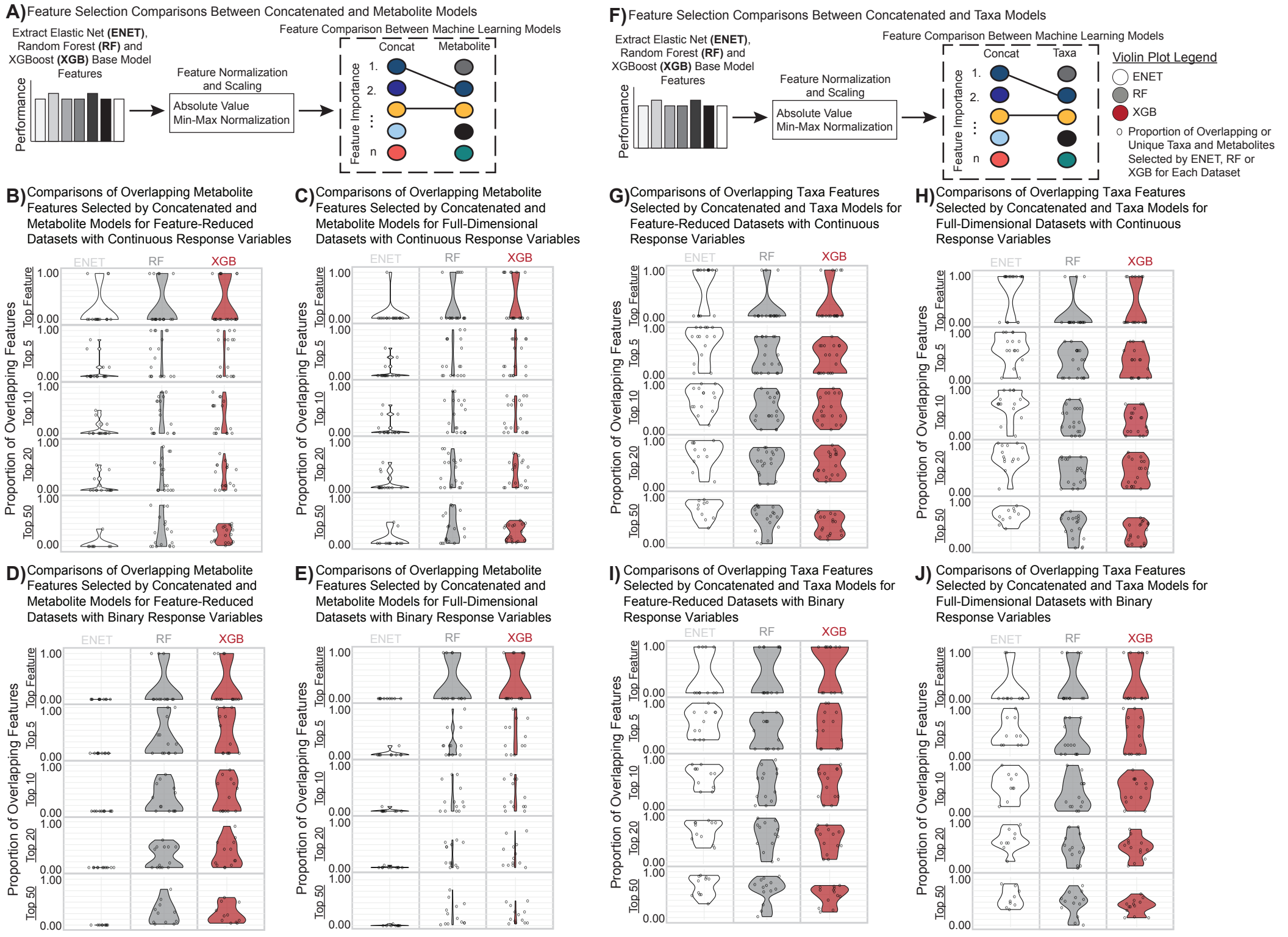
A) Feature Selection Comparisons Between Concatenated and Metabolite Models
Extract Elastic Net (ENET), Random Forest (RF) and XGBoost (XGB) Base Model Features
Performance
Feature Normalization and Scaling
Absolute Value Min-Max Normalization
Feature Comparison Between Machine Learning Models
Concat
Metabolite
Feature Importance
1.
2.
n
B) Comparisons of Overlapping Metabolite Features Selected by Concatenated and Metabolite Models for Feature-Reduced Datasets with Continuous Response Variables
C) Comparisons of Overlapping Metabolite Features Selected by Concatenated and Metabolite Models for Full-Dimensional Datasets with Continuous Response Variables
D) Comparisons of Overlapping Metabolite Features Selected by Concatenated and Metabolite Models for Feature-Reduced Datasets with Binary Response Variables
E) Comparisons of Overlapping Metabolite Features Selected by Concatenated and Metabolite Models for Full-Dimensional Datasets with Binary Response Variables
F) Feature Selection Comparisons Between Concatenated and Taxa Models
Extract Elastic Net (ENET), Random Forest (RF) and XGBoost (XGB) Base Model Features
Performance
Feature Normalization and Scaling
Absolute Value Min-Max Normalization
Feature Comparison Between Machine Learning Models
Concat
Taxa
Feature Importance
1.
2.
n
Violin Plot Legend
ENET
RF
XGB
Proportion of Overlapping or Unique Taxa and Metabolites Selected by ENET, RF or XGB for Each Dataset
G) Comparisons of Overlapping Taxa Features Selected by Concatenated and Taxa Models for Feature-Reduced Datasets with Continuous Response Variables
H) Comparisons of Overlapping Taxa Features Selected by Concatenated and Taxa Models for Full-Dimensional Datasets with Continuous Response Variables
I) Comparisons of Overlapping Taxa Features Selected by Concatenated and Taxa Models for Feature-Reduced Datasets with Binary Response Variables
J) Comparisons of Overlapping Taxa Features Selected by Concatenated and Taxa Models for Full-Dimensional Datasets with Binary Response Variables
ENET
RF
XGB
Proportion of Overlapping Features
Top Feature
Top 5
Top 10
Top 20
Top 50
1.00
0.00

717 **Figure 8. Feature Selection Comparisons Between Concatenated (Concat) and Individual**
718 **(Metabolomics/Taxa) Elastic Net (ENET), Random Forest (RF) and XGBoost (XGB) Models.** The pipeline
719 for extracting feature importance metrics and performing comparisons between concatenated and metabolites
720 models are represented in **A)**. Feature Importance values for ENET, RF and XGB were extracted for each cross-
721 validation step. The absolute value was taken for each value and min-max normalization was performed. The
722 overall average for each feature was then used as the metric for feature importance. See **Methods** for more
723 details. Comparisons for the metabolites selected by concatenated and metabolomics models for feature-
724 reduced datasets with continuous response variables are represented by **B)**. Comparisons for the metabolites
725 selected by concatenated and metabolomics models for full-dimensional datasets with continuous response
726 variables are represented by **C)**. Comparisons for the metabolites selected by concatenated and metabolomics
727 models for feature-reduced datasets with binary response variables are represented by **D)**. Comparisons for the
728 metabolites selected by concatenated and metabolomics models for full-dimensional datasets with binary
729 response variables are represented by **E)**. The pipeline for extracting feature importance metrics and performing
730 comparisons between concatenated and metabolites models are represented in **F)** (See details above (**A**) and
731 in **Methods**). Comparisons for the taxa selected by concatenated and taxa models for feature-reduced datasets
732 with continuous response variables are represented by **G)**. Comparisons for the taxa selected by concatenated
733 and taxa models for full-dimensional datasets with continuous response variables are represented by **H)**.
734 Comparisons for the taxa selected by concatenated and taxa models for feature-reduced datasets with binary
735 response variables are represented by **I)**. Comparisons for the taxa selected by concatenated and taxa models
736 for full-dimensional datasets with binary response variables are represented by **J)**. For each analysis, top
737 features for ENET, RF and XGB were binned into 5 levels – top feature (i.e., features with highest feature
738 importance values), top 5 features, top 10 features, top 20 features and top 50 features. For each bin,
739 comparisons for the features selected by concatenated and individual (metabolomics and taxa) omics models
740 for ENET, RF and XGB were performed to identify joint and unique features. The distribution of dataset
741 proportions for overlapping and unique features are represented by violin plots for panels **B-E** and **G-J**.

742

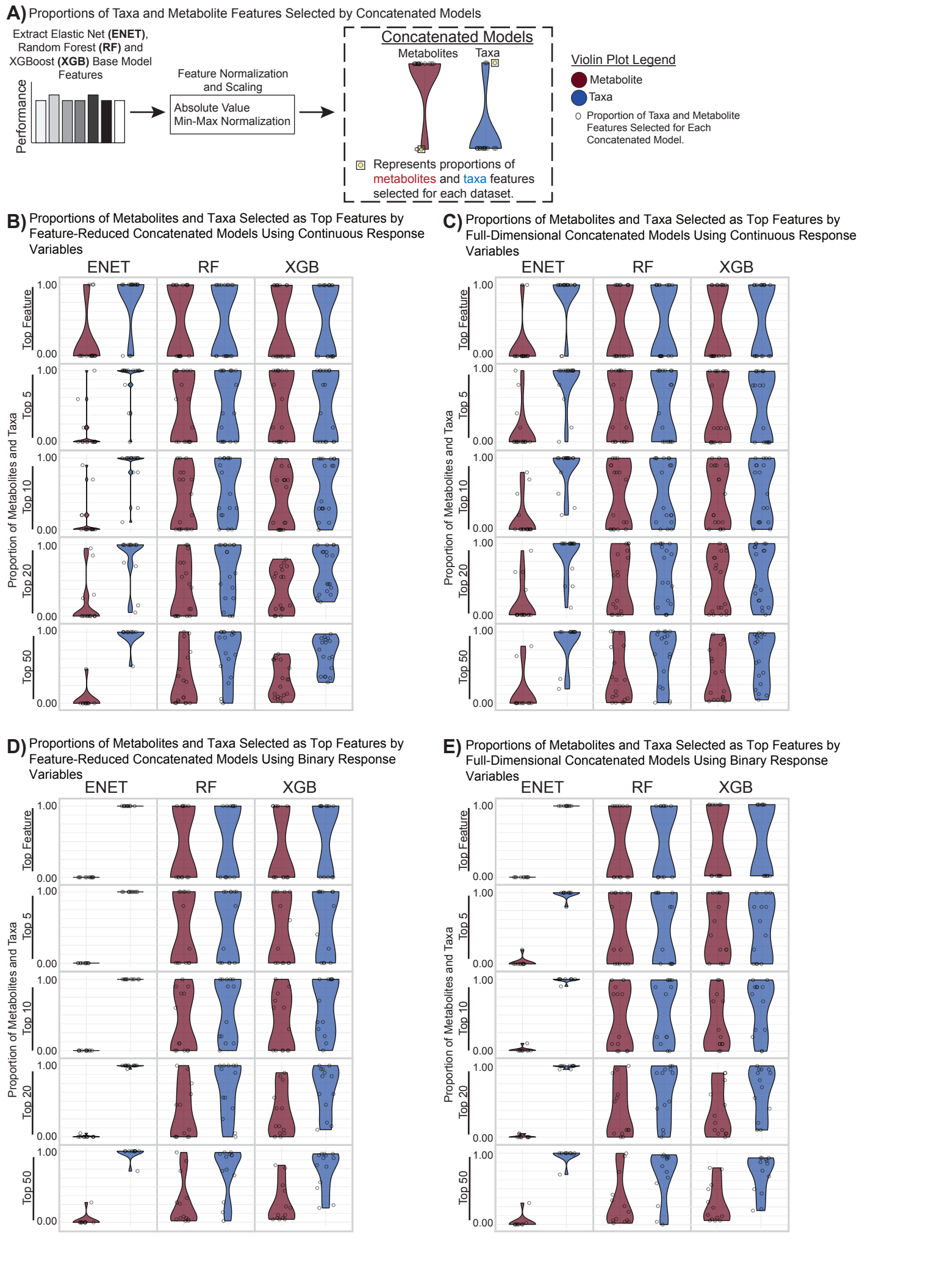
A) Proportions of Taxa and Metabolite Features Selected by Concatenated Models
Extract Elastic Net (ENET), Random Forest (RF) and XGBoost (XGB) Base Model Features
Performance
Feature Normalization and Scaling
Absolute Value
Min-Max Normalization
Concatenated Models
Metabolites
Taxa
Represents proportions of metabolites and taxa features selected for each dataset.
Violin Plot Legend
Metabolite
Taxa
Proportion of Taxa and Metabolite Features Selected for Each Concatenated Model.
B) Proportions of Metabolites and Taxa Selected as Top Features by Feature-Reduced Concatenated Models Using Continuous Response Variables
C) Proportions of Metabolites and Taxa Selected as Top Features by Full-Dimensional Concatenated Models Using Continuous Response Variables
D) Proportions of Metabolites and Taxa Selected as Top Features by Feature-Reduced Concatenated Models Using Binary Response Variables
E) Proportions of Metabolites and Taxa Selected as Top Features by Full-Dimensional Concatenated Models Using Binary Response Variables
ENET
RF
XGB
Proportion of Metabolites and Taxa
Top Feature
Top 5
Top 10
Top 20
Top 50
1.00
0.00

743 **Supplemental Figure 3: Proportions of Taxa and Metabolite Features Selected by Concatenated Models.**
744 The pipeline for extracting feature importance metrics and calculating proportions of the top features that are
745 metabolites and taxa selected by the concatenated models are represented by **A)**. The Proportions of taxa and
746 metabolite features selected by ENET, RF and XGB for concatenated feature-reduced datasets with continuous
747 response variable are shown in **B)**. The Proportions of taxa and metabolite features selected by ENET, RF and
748 XGB for concatenated full-dimensional datasets with continuous response variable are shown in **C)**. The
749 Proportions of taxa and metabolite features selected by ENET, RF and XGB for concatenated feature-reduced
750 datasets with binary response variable are shown in **D)**. The Proportions of taxa and metabolite features selected
751 by ENET, RF and XGB for concatenated full-dimensional datasets with binary response variable are shown in
752 **E)**. The distribution of proportions for each dataset are represented as violin plots. For each analysis, top features
753 for ENET, RF and XGB were binned into 5 levels – top feature (i.e., features with highest feature importance
754 values), top 5 features, top 10 features, top 20 features and top 50 features. The red violin plot represents
755 metabolomics proportions for each dataset and the blue violin plot represents the taxa proportions for each
756 dataset. These violin plot values are inverse proportional for each dataset, so that if the proportion of metabolites
757 for Dataset A = 1, then the proportion of taxa for Dataset A = 0.

758

759

Supplemental File 1: Current Standard and Published Integration Strategies for Metagenomic and Metabolomics Multi-omics Datasets

The high dimensionality and sparsity of microbiome data further complicates multi-omics integration, negatively impacting model stability and generalizability [1,2]. Given these complexities, feature selection and dimensionality reduction can be critical for improving model interpretability, reducing overfitting, and enhancing the reproducibility of selected microbial and metabolic features. Commonly used methods for feature selection include Elastic Net, Recursive Feature Elimination (RFE), and Random Forest-based selection, while dimensionality reduction techniques such as Principal Component Analysis (PCA) and Partial Least Squares (PLS) are often employed to improve model efficiency and interpretability [3-5]. However, little is known about how feature reduction impacts prediction model performance in multi-omics integration. While deep learning models have been explored for microbiome data integration, their lack of interpretability makes them less desirable for biomarker identification.

Several studies have utilized different machine learning and integration strategies, yet no consensus exists on the optimal approach. For instance, Franzosa et al. 2019 [6] used concatenated metabolomics and species data to classify Control versus IBD, as well as the diseases subclasses (UC and CD). Li et al. 2017 [7] implemented concatenated random forest models to distinguish healthy controls from hypertension patients. Gao et al. 2020 [8] applied concatenated logistic regression to predict 30-day survival in patients with alcoholic hepatitis using microbial pathway and metabolite data. Yachida et al. 2019 [9] developed random forest and LASSO logistic regression classifiers to discriminate colorectal cancer cases from healthy controls. Meanwhile, Ghaemi et al. 2018 [10] objectively tested five machine learning models before selecting Elastic Net for integrating seven different omics datasets using stacked generalization. Mallick et al. 2023 [11] compared concatenated and stacked generalization approaches, finding that Bayesian Additive Regression Trees (BART) combined with Non-Negative Least Squares (NNLS) performed best for the tested microbiome datasets. While Partial Least Squares (PLS) regression has not been extensively explored for microbiome ensemble predictors, its potential in this domain warrants investigation due to its ability to handle collinear and high-dimensional data effectively. Given the challenges of multi-omics integration, incorporating PLS as a meta-

learner in stacked generalization may enhance predictive performance by leveraging shared variance across omics layers, reducing overfitting, and improving feature selection consistency.

References

1. Lutz KC, Jiang S, Neugent ML, *et al.* A Survey of Statistical Methods for Microbiome Data Analysis. Front Appl Math Stat. 2022;8:884810.
2. Pan, A. Statistical analysis of microbiome data: The challenge of sparsity. Current Opinion in Endocrine and Metabolic Research. 2021 Aug;19:35-40.
3. Greener JG, Kandathil SM, Moffat L, et al. A guide to machine learning for biologists. Nature Reviews Molecular Cell Biology. 2022 Jan;23(1):40-55.
4. Li Y, Wu FX, Ngom A. A review on machine learning principles for multi-view biological data integration. Briefings in Bioinformatics. 2018 Mar 1;19(2):325-340.
5. Ghannam RB, Techtmann SM. et al. Machine learning applications in microbial ecology, human microbiome studies, and environmental monitoring. Computational and Structural Biotechnology Journal. 2021 Jan 27;19:1092-1107.
6. Franzosa EA, Sirota-Madi A, Avila-Pacheco J, et al. Gut microbiome structure and metabolic activity in inflammatory bowel disease. Nature Microbiology. 2019 Feb;4(2):293-305.
7. Li J, Zhao F, Wang Y, et al. Gut microbiota dysbiosis contributes to the development of hypertension. Microbiome. 2017 Feb 1;5(1):14.
8. Gao B, Duan Y, Lang S, et al. Functional Microbiomics Reveals Alterations of the Gut Microbiome and Host Co-Metabolism in Patients With Alcoholic Hepatitis. Hepatology Communications. 2020 Jun 19;4(8):1168-1182.
9. Yachida S, Mizutani S, Shiroma H, et al. Metagenomic and metabolomic analyses reveal distinct stage-specific phenotypes of the gut microbiota in colorectal cancer. Nature Medicine. 2019 Jun;25(6):968-976.
10. Ghaemi MS, DiGiulio DB, Contrepois K, et al. Multiomics modeling of the immunome, transcriptome, microbiome, proteome and metabolome adaptations during human pregnancy. Bioinformatics. 2019 Jan 1;35(1):95-103.
11. Mallick H, Porwal A, Saha S, et al. An integrated Bayesian framework for multi-omics prediction and classification. Statistics in Medicine. 2024 Feb 28;43(5):983-1002.

Supplemental File 2: Extended Methods

Metagenomic Shotgun Sequencing Processing: Raw FASTQ files were obtained from the original studies [1–4] and processed using fastp v0.23.2 for quality filtering, adapter trimming, and deduplication [5]. Host DNA was removed using Bowtie v2.3.5 [6], which aligned human reads to the human reference genome (Genome Reference Consortium Build 38). Taxonomic classification and relative abundance estimates were generated using Kraken v2.1.1 and Bracken v2.8 [7-8], with the Genome Taxonomy Database (GTDB v207) [9-10] as the reference. Samples with fewer than 50,000 reads were excluded from downstream analyses. Taxonomic abundance data were obtained from the "genera.tsv" and "species.tsv" files provided by Müller et al., [11].

Metabolomics Data Processing: The metabolomics data collected across studies vary in analytical platforms, technologies, and normalization procedures. As a result, normalization approaches and control strategies differ between datasets. Metabolite compound identifiers were not altered from their original publications [1-4] and are available in the **"**mtb.tsv**"** files provided by Müller et al., [11].

Metadata: Metadata was extracted from the original studies [1-4] and compiled in the **"**metadata.tsv**"** file from Muller et al., [11]. Additional details on data processing can be found at: https://github.com/borenstein-lab/microbiome-metabolome-curated-data/wiki5.

Data Processing for the Integrated Analysis

Processed data files, including "mtb.tsv" (metabolites), "genera.tsv" (genus-level taxa), "species.tsv" (species-level taxa), and "metadata.tsv", were further refined for downstream analysis. Taxonomic data at the genus and species levels were concatenated for each dataset, and taxa with an overall abundance below 0.001 across all samples were removed. To facilitate automated parsing in the integrative analysis, an "m__" prefix was added to metabolite names, and a "t__" prefix was added to taxonomic features. For metabolite differential intensity analysis, Limma was applied, which employs linear modeling and empirical Bayes methods to identify significant differences while adjusting for multiple testing [12]. For taxonomic differential analysis, the Wilcoxon rank-sum test was used to compare taxa abundance across experimental groups.

Franzosa Data: Metabolite data were $\log_2$-transformed to normalize distributions. A new response variable, "disease_status," was created to classify samples as either Control or Irritable Bowel Disease (IBD) (Ulcerative Colitis (UC) and Crohn's Disease (CD)). Additionally, Fecal Calprotectin (Fp) was $\log_2$-transformed to reduce skewness. Three independent comparisons were performed, including Control vs. CD, Control vs. IBD

(combined CD and UC), and Control vs. UC. Each comparison included two continuous variables (Age and Fp) and a binary classification (Control vs. Disease). Metabolite differential intensity analysis was conducted using Limma[12], and metabolites with a $\log_2$ fold-change and an adjusted p-value < 0.05 were retained. For taxonomic differential analysis, the Wilcoxon rank-sum test was applied, selecting taxa with an adjusted p-value < 0.05 (corrected for multiple testing using Benjamini-Hochberg). Metabolite, taxonomy, and response variables were concatenated for both the original dataset and differentially expressed features, and samples with missing values were removed. In total, 9 response variables were analyzed for both datasets, yielding 18 datasets **(Tables 1–2)**.

Erawijantari Data: Metabolite data were $\log_2$-transformed, and metabolites with an adjusted p-value < 0.05 (corrected for multiple testing using Benjamini-Hochberg) and a $\log_2$ fold-change were retained for further analysis. For taxonomic differential analysis, the Wilcoxon rank-sum test was used to compare taxa abundance between Control and Gastrectomy groups, with taxa selected based on an adjusted p-value < 0.05 (corrected for multiple testing). The dataset included three continuous variables (Age, Total Cholesterol, and Glucose) and three binary classifications (No Alcohol vs. Alcohol, Female vs. Male, and Control vs. Gastrectomy). Metabolite, taxonomy, and response variables were concatenated, and samples with missing values were removed. In total, 6 response variables were analyzed for both datasets, resulting in 12 datasets **(Tables 1–2)**.

Wang Data: Metabolites with an adjusted p-value < 0.05 were retained for further analysis. Taxonomic differential analysis was performed using the Wilcoxon rank-sum test to compare taxa abundance between Control and Kidney Disease groups, selecting taxa with an adjusted p-value < 0.05 (corrected for multiple testing). Creatinine was $\log_2$-transformed to reduce skewness. The dataset included five continuous variables (Age, BMI, Creatinine, eGFR, and Urea) and two binary classifications (Female vs. Male and Control vs. Kidney Failure). Metabolite, taxonomy, and response variables were concatenated, and samples with missing values were removed. In total, 7 response variables were analyzed for both datasets, resulting in 14 datasets **(Tables 1–2)**.

Yachida Data: Metabolite data were $\log_2$-transformed, and metabolites with an adjusted p-value < 0.05 were retained. Taxonomic differential analysis was conducted using the Wilcoxon rank-sum test to compare taxa abundance between Control and Disease groups, selecting taxa with an adjusted p-value < 0.05 (corrected for multiple testing). Samples were stratified into five comparison groups: All Samples, Control vs. Multiple Polyploid Adenomas (MP) & Colorectal Cancer (CRC), Control vs. MP & Stage 0 (early-stage CRC), Control vs. Stage 1

& 2 CRC, and Control vs. Stage 3 & 4 CRC. Additionally, Alcohol and Brinkman Index were $\log_2$-transformed to normalize distributions. The dataset included four continuous variables (Age, Alcohol, BMI, and Brinkman Index) and five binary classifications (Female vs. Male, Control vs. MP & CRC, Control vs. MP & Stage 0 CRC, Control vs. Stage 1 & 2 CRC, and Control vs. Stage 3 & 4 CRC). Metabolite, taxonomy, and response variables were concatenated, and samples with missing values were removed. In total, 9 response variables were analyzed for both datasets, resulting in 18 datasets **(Tables 1–2)**.

Overview of Multi-omics Integrative Analysis

The integrative analysis was developed using a custom in-house script that is readily available at https://github.com/suziepalmer10/Multiomics-Integrative-Pipeline/tree/main. The accepted data format is a concatenated matrix containing the response variable, stratified variable (if specified), metabolomics data (denoted by "m__"), and taxonomy data (denoted by "t__"). For each dataset run, users must provide the desired machine learning model script (e.g., random_forest.R), the file path where the automated pipeline script is stored, the name of the data file, the study name for labeling output files, the type of analysis (binary or continuous), the name of the response variable, the name of the stratification variable (if applicable), the proportion of training data, the number of folds, and the number of repeats for cross-validation. The packages tidyverse 2.0.0 and argparse 2.2.3 were used to parse and pre-process the data for this integrative analysis[13].

Upon completion, the script generates four output files, including performance metrics for the five integrated models (concatenated, averaged stacked, weighted NNLS, Lasso stacked, and PLS) and two single-omics models (metabolomics and taxonomy) for the selected machine learning method (Elastic Net, XGBoost, or Random Forest). Additionally, an R Data file, metadata output, and a bar graph comparing validation and testing performance are provided. Performance metrics for continuous data include Root Mean Squared Error (RMSE), Mean Absolute Error (MAE), and R^2, while binary classification performance metrics include Accuracy, Area Under the Receiver Operating Characteristic Curve (AUROC), and Kappa. More details are available in the user guide at https://github.com/suziepalmer10/Multiomics-Integrative-Pipeline/tree/main. For the integrative analysis, AUROC is calculated using pROC 1.18.0 and Kappa is calculated using irr 0.84.1[14-15].

For this analysis, each dataset (as described above and presented in **Tables 1–2**) was processed through the Integrated Pipeline using standard Elastic Net, Random Forest, and XGBoost scripts, generating 21 models per dataset. The data was split into 80% training and 20% testing, and three repeats of five-fold cross-

validation were performed. To ensure both generalizability and reproducibility, the seed was varied for each fold using set.seed(repeat_ * fold). Performance was evaluated on both validation and test sets. Grid search with a predefined grid was used for Elastic Net, Random Forest, and XGBoost.

Elastic Net Overview and Grid: The Elastic Net algorithm estimates β coefficients to minimize the error term $L(\beta) = \|Y - X\beta\|^2$, where X represents the data matrix (concatenated, taxonomy, or metabolomics), and Y represents the response variable. The regularization penalty combines L_1 (Lasso) and L_2 (Ridge) penalties. The penalty term added to the loss function is $\lambda(\alpha \sum|\beta_j| + (1-\alpha)\sum \beta_j^2)$, where $\sum |\beta_j|$ represents the L_1 penalty, $\sum \beta_j^2$ represents the L_2 penalty, λ determines the overall regularization strength, and α controls the balance between L_1 and L_2 regularization. For this analysis, the caret 6.0-93 and glmnet 4.1-6 R packages were used[16-17]. A grid search was conducted using alpha = seq(0, 1, by = 0.1) and lambda = seq(0.01, 1, length = 10). A binomial family was used for binary responses, while a Gaussian family was used for continuous response variables.

Random Forest Overview and Grid: The Random Forest algorithm constructs an ensemble of decision trees to enhance prediction accuracy and reduce overfitting. Each tree is trained on a bootstrapped sample of the data, and predictions are obtained via averaging (for regression) or majority voting (for classification). To introduce randomness and reduce feature correlation, Random Forest selects a subset of features at each split. For this analysis, the caret and randomForest 4.7-1.1 R packages were used[16,18]. The model was trained to minimize prediction error and the key tuning parameter, mtry, was used to determine the number of randomly selected features considered at each split. A grid search was conducted with mtry = seq(2, sqrt(ncol(trainData) - 1), by = 10). For classification tasks, the model used Gini impurity for node splitting, while for regression, the mean absolute error (MAE) criterion was applied.

XGBoost Overview and Grid: XGBoost is an optimized gradient boosting algorithm that iteratively refines weak learners to minimize the loss function. It incorporates regularization to mitigate overfitting and utilizes efficient parallel processing for computational efficiency. For this analysis, the caret and xgboost 1.7.8.1 R packages were used[16,19]. Grid search was performed using the following parameters: nrounds = c(100, 150, 200), max_depth = c(4, 6, 8, 10), eta = c(0.01, 0.1, 0.2), colsample_bytree = c(0.6, 0.8, 1), subsample = c(0.6, 0.8, 1), gamma = 0, min_child_weight = 1. For binary classification tasks, a log-loss objective function was used, whereas for regression tasks, the squared error loss function was applied.

Data integration using direct concatenation: To integrate taxa and functional data using direct concatenation, we will horizontally concatenate the two matrices, where A represents taxonomy data and B represents functional data. Both matrices share the same number of rows (m), corresponding to the samples and disease phenotype that is used as the response variable. However, these matrices differ in the number of columns, n_A, which represents the number of taxa and, n_B, which represents the number of functional data (i.e., metabolites). Mathematically, let $A = \begin{pmatrix} a_{11} & \cdots & a_{1n_A} \\ \vdots & \ddots & \vdots \\ a_{m1} & \cdots & a_{mn_A} \end{pmatrix}$ and $B = \begin{pmatrix} b_{11} & \cdots & b_{1n_B} \\ \vdots & \ddots & \vdots \\ b_{m1} & \cdots & b_{mn_B} \end{pmatrix}$. Concatenation results in C, where $C = [A|B]$. This creates a unified matrix, where $C \in \mathbb{R}^{m\times(n_A+n_B)}$, which enables the integration of the distinct datatypes while preserving the sample structure. We then use the combined matrix, C, for machine learning model development using Elastic Net, XGBoost and Random Forest algorithms.

Data integration using averaged stacking of the predictors: Data integration using averaged stacking combines predictions from individual machine learning models (Random Forest, XGBoost or Elastic Net) for each dataset (taxonomy and metabolomics) into a single, averaged prediction for each sample. For averaged stacking, let $P_A \in \mathbb{R}^{m\times 1}$ represent predictions from a machine learning model trained on taxonomy data, A and let $P_B \in \mathbb{R}^{m\times 1}$ represent predictions from a machine learning model trained on functional data. Let m represent the number of samples and response variables that are shared across both datasets. The averaged stacking prediction, P_{avg}, for each sample is computed as $P_{Avg} = \frac{1}{2}(P_A + P_B)$, where $P_{Avg} \in \mathbb{R}^{m\times 1}$ represents the integration prediction vector across all samples.

Data integration using weighted non-negative least squares (NNLS): Data integration using weighted nnls combines predictions from each model by assigning weights to minimize the error between the combined predictions and the observed values, with the constraint that weights are non-negative. As previously described above, let $P_A \in \mathbb{R}^{m\times 1}$ and $P_B \in \mathbb{R}^{m\times 1}$, represent predictions from a machine learning model trained on taxa data, A, and functional data, B. Let $y \in \mathbb{R}^{m\times 1}$ represent response variables and let w_A and w_B represent non-negative weights assigned to P_A and P_B. The combined prediction $P_{NNLS} = w_A P_A + w_B P_B$, where the weights w_A and w_B are determined by solving the following optimization problem, where $\min_{w_A, w_B \geq 0} \|y - (w_A P_A + w_B P_B)\|^2$. The nnls 1.5 package was used for non-negative least squares analysis[20].

Data integration using least absolute shrinkage and selection operator (LASSO) stacked generalization: Data integration using LASSO combines predictions by assigning weights to minimize the error between the combined prediction and the observed values while enforcing sparsity in the rights through L_1 regularization. As previously described, let $P_A \in \mathbb{R}^{m\times 1}$ and $P_B \in \mathbb{R}^{m\times 1}$, represent predictions from a machine learning model trained on taxa data, A, and functional data, B, and let $y \in \mathbb{R}^{m\times 1}$ represent response variables. For LASSO, let w_A and w_B represent weights assigned to P_A and P_B. The combined prediction, $P_{LASSO} = w_A P_A + W_B P_B$, where the weights w_A and w_B are determined by solving the following optimization problem using L_1 regularization: $\min_{w_A, w_B \geq 0} \|y - (w_A P_A + w_B P_B)\|^2 + \lambda(|w_A| + |w_B|)$, where λ is the weight of the L_1 regularization term and controls solution sparsity. The glmnet 4.1-6 package was using for LASSO[17].

Data integration using partial least squares (PLS): PLS is a regression method that combines the predictors from separate machine learning models by projecting the predictors into a lower dimensional space to maximize the covariance between the predictors and the response variables. This integrative method can handle multicollinearity and captures the shared variation between different datatypes. PLS operates in three stages. The first stage is latent component extraction, where PLS identifies latent components, T, by projecting the combined predictor matrix, P, onto a set of weight vectors that maximize the covariance between the latent components, T, and the response variable, y. Mathematically, $T = PW$, and as previously described, let $P_A \in \mathbb{R}^{m\times 1}$ and $P_B \in \mathbb{R}^{m\times 1}$, represent predictions from a machine learning model trained on taxa data, A, and functional data, B, and let $y \in \mathbb{R}^{m\times 1}$ represent response variables. Let $P = [P_A | P_B] \in \mathbb{R}^{m\times 2}$, represent the concatenated matrix of predictors. Let $T \in \mathbb{R}^{m\times k}$ represent the latent variables extracted by P, where k represents the number of components. Let $W \in \mathbb{R}^{2\times k}$ represent a weight matrix that defines the linear combination between P_A and P_B. The next stage of PLS is to create a linear regression of the response variable. This is accomplished following extraction of latent components, T, and the response variable, y, are then modeled as a linear function of T. Mathematically, $y = TC + \varepsilon$, where $C \in \mathbb{R}^{k\times 1}$ represent regression coefficients for T to predict y and ε represents the residual error term. The final stage is to combine the projection and the regression stages, which can be mathematically represented as $y_{PLS} = PWC$. The pls 2.8-4 package[21] was used for partial least squares model generation.

Performance Heatmap Generation: Following completion of each machine learning model (Elastic Net, XGBoost or Random Forest), the performance metrics mean and standard deviation are provided as an output file. The average AUROC values for binary response variables and the average RMSE values for the continuous response variables were extracted for each dataset and model using an in-house script. Following creation of the Heatmap using the Complexheatmap R package[22, 23], the top 3 performing models across each dataset for Elastic Net (if completed), Random Forest and XGBoost. These are represented by the "*", "**", and "***", and do not include the single-omics performance metrics. For some of the datasets, the Elastic Net model was unable to run due to insufficient grid and/or the likely need for further data processing which we decided not to further optimize for this study.

Performance Pie Charts: The R package ggplot2 3.4.1 was used to create the performance heatmaps for Figures 2-3 and Supplemental Figures 1-2[24]. These metrics were calculated by quantifying the number of models for each dataset that were part of the top 3 performing models (represented as '*", "**" and "***") (described above for Performance Heatmap Generation).

Feature Importance: Feature importance values were extracted from Elastic Net, XGBoost and Random Forest across all 15 cross-validation models. For Elastic Net, feature importance is accessed through the magnitude of its regression coefficients, where larger absolute values reflect greater predictive contributions. For random forest mean decrease in impurity (MDI) is applied to quantify feature importance and reflects the reduction in impurity achieved by splitting on a given feature, averages across all decision trees generated. For XGBoost, the Gain metric is used to access how effectively a feature improves the objective function by reducing prediction error during tree splits.

Feature importance values were extracted from Elastic Net, XGBoost and Random Forest across all 15 cross-validation models. Since different metrics were used to quantify feature importance across Elastic Net, Random Forest and XGBoost models, we decided to take the absolute value of each variable and perform min-max normalization (data scaled between 0 and 1) for each model. Mathematically, let i denote the feature ($i = \{1, 2 \dots n\}$), where n is the total number of features. Let j denote the model ($j = \{1,2 \dots C\}$), where C represents the number of folds and repeats from 5-fold cross validation. Let $|S_{i,j}|$ represent the absolute value for the importance score of feature i in model j. Next min-max normalization, $N_{i,j}$, for feature i for model j is calculated

by $N_{i,j} = \frac{|S_{i,j}| - min_k(|S_{k,j}|)}{max_k(|S_{k,j}|) - min_k(|S_{k,j}|)}$, where k indexes over all features in model j. I next compute the averaged normalized importance for each feature across all models, $\overline{N}_i = \frac{1}{C}\sum_{j=1}^{C} N_{i,j}$. This allows for direct comparison between features in each model.

References

1. Franzosa EA, Sirota-Madi A, Avila-Pacheco J, et al. Gut microbiome structure and metabolic activity in inflammatory bowel disease. Nature Microbiology. 2019 Feb;4(2):293-305.
2. Yachida S, Mizutani S, Shiroma H, et al. Metagenomic and metabolomic analyses reveal distinct stage-specific phenotypes of the gut microbiota in colorectal cancer. Nature Medicine. 2019 Jun;25(6):968-976.
3. Erawijantari PP, Mizutani S, Shiroma H, et al. Influence of gastrectomy for gastric cancer treatment on faecal microbiome and metabolome profiles. Gut. 2020 Aug;69(8):1404-1415.
4. Wang X, Yang S, Li S, et al. Aberrant gut microbiota alters host metabolome and impacts renal failure in humans and rodents. Gut. 2020 Dec;69(12):2131-2142.
5. Chen S, Zhou Y, Chen Y, et al. Fastp: an ultra-fast all-in-one FASTQ preprocessor. Bioinformatics. 2018. 2018 Sep 1;34(17):i884-i890.
6. Langmead B, Salzberg SL. Fast gapped-read alignment with Bowtie 2. Nature Methods. 2012 Mar 4;9(4):357-9.
7. Wood DE, Lu J, Langmead B. Improved metagenomic analysis with Kraken 2. Genome Biology. 2019 Nov 28;20(1):257.
8. Lu J, Breitwieser FP, Thielen P, et al. Bracken: estimating species abundance in metagenomics data. PeerJ Computer Science. 2017 Jan;3:e104.
9. Parks, D. H. *et al.* GTDB: an ongoing census of bacterial and archaeal diversity through a phylogenetically consistent, rank normalized and complete genome-based taxonomy. Nucleic Acids Res. 2022 Jan 7;50(D1):D785-D794.
10. Youngblut, N. D., Youngblut, N. D., Ley, R. E. & Ley, R. E. Struo2: efficient metagenome profiling database construction for ever-expanding microbial genome datasets. PeerJ. 2021 Sep 16;9:e12198.
11. Muller E, Algavi YM, Borenstein E. The gut microbiome-metabolome dataset collection: a curated resource for integrative meta-analysis. Npj Biofilms and Microbiomes. 2022 Oct 15;8(1):79.
12. Ritchie ME, Phipson B, Wu D, et al. Limma powers differential expression analyses for RNA-sequencing and microarray studies. Nucleic Acids Research. 2015 Apr 20;43(7):e47.
13. Wickham H, Averick M, Bryan J, et al. Welcome to the Tidyverse. Journal of Open Source Software. 2019 Nov; 4(43):1686.
14. Robin, X. *et al.* PROC: an open-source package for R and S+ to analyze and compare ROC curves. *BMC Bioinformatics* (2011) doi:10.1186/1471-2105-12-77.
15. Gamer M, Lemon J, Singh IFP. Irr: Various Coefficients of Interrater Reliability and Agreement. https://CRAN.R-project.org/package=irr. (27 June 2025, date last accessed).
16. Kühn M. Building Predictive Models in R Using the caret Package. Journal of Statistical Software. 2008 Nov;28(5):1-26.17.
17. Friedman J, Hastie T, Tibshirani R. et al. Regularization Paths for Generalized Linear Models via Coordinate Descent. Journal of Statistical Software. 2010 Aug;33(1):1-22.
18. Liaw A, Wiener MC. Classification and Regression by randomForest. R News. 2002 Dec;2:18-22.
19. Chen T, Guestrin C. XGBOOST: A Scalable Tree Boosting System. KDD '16: Proceedings of the 22nd ACM SIGKDD International Conference on Knowledge Discovery and Data Mining. 2016 Aug 13; 785-794.
20. Mullen KM, van Stokkum IHM. nnls: The Lawson-Hanson Algorithm for Non-Negative Least Squares (NNLS). https://rdrr.io/cran/nnls/ (27 June 2025, date last accessed).
21. Mevik B-H, Wehrens R. The pls Package: Principal Component and Partial Least Squares Regression in R. Journal of Statistical Software. 2007 Jan;18:1–23.
22. Gu Z. Complex heatmap visualization. iMeta. 2022 Sept;3(1):e43.
23. Gu Z, Eils R, Schlesner M. Complex heatmaps reveal patterns and correlations in multidimensional genomic data. Bioinformatics. 2016 Sep 15;32(18):2847-9.
24. Valero-Mora PM, Valero-Mora PM. Ggplot2: Elegant Graphics for Data Analysis. Journal of Statistical Software, Book of Reviews. 2010 Jul;35(1):1-3.